REPORT 1232

A THEORETICAL AND EXPERIMENTAL INVESTIGATION OF THE LIFT AND DRAG CHARACTERISTICS OF HYDROFOILS AT SUBCRITICAL AND SUPERCRITICAL SPEEDS [1]

By Kenneth L. Wadlin, Charles L. Shuford, Jr., and John R. McGehee

SUMMARY

A theoretical and experimental investigation at subcavitation speeds was made of the effect of the free-water surface and rigid boundaries on the lift and drag of an aspect-ratio-10 hydrofoil at both subcritical and supercritical speeds and of an aspect-ratio-4 hydrofoil at supercritical speeds. For the aspect-ratio-10 hydrofoil, tests were made in Langley tank no. 1 and Langley tank no. 2 at 0.84 and 3.84 chords submergence at subcavitation speeds from 5 to 45 fps corresponding to Reynolds numbers from 0.18 $\times$ 10^6 to 1.64 $\times$ 10^6. For the aspect-ratio-4 hydrofoil, tests were made in Langley tank no. 2 at 0.59, 1.09, 2.09, 3.09, and 4.09 chords submergence at subcavitation speeds from 15 to 35 fps corresponding to Reynolds numbers from 0.873 $\times$ 10^6 to 2.04 $\times$ 10^6.

Approximate theoretical solutions for the effects of the free-water surface and rigid boundaries on lift and drag at supercritical speeds are developed. An approximate theoretical solution for the effects of these boundaries on drag at subcritical speeds is also presented. The agreement between theory and experiment at both supercritical and subcritical speeds is satisfactory for engineering calculations of hydrofoil characteristics from aerodynamic data.

The experimental investigation indicated no appreciable effect of the limiting speed of wave propagation on lift-curve slope or angle of zero lift. It also showed that the increase in drag as the critical speed is approached from the supercritical range is gradual. This result is contrary to the abrupt increase at the critical speed predicted by theory.

INTRODUCTION

Airfoils and hydrofoils operate in fluids which differ principally in density and viscosity, properties that are readily treated by the concept of Reynolds number. Since such is true, the vast amount of aerodynamic data already accumulated becomes available for use in predicting hydrofoil characteristics. The airfoil, however, generally operates in an essentially infinite medium, whereas hydrofoil applications usually require operation in a limited medium, that is, in the proximity of the water surface. Aside from the effects of cavitation then, the principal difference between airfoil and hydrofoil applications is one of boundaries.

In restricted areas such as shallow harbors, canals, and towing tanks, other boundaries are present besides the water surface, that is, the bottom and sides. Naturally these boundaries also influence the characteristics of a hydrofoil, and their effects must be evaluated in order to use aerodynamic data for the prediction of the characteristics of hydrofoils under such conditions.

In addition to the reflective influence of the bottom and sides, the finite depth of water limits the speed of propagation of the transverse waves generated by the hydrofoil. This change in flow causes the lift and drag characteristics to be different at speeds below this limiting speed or critical speed than they are above it.

In the present report available aerodynamic and hydrodynamic theories have been applied to develop an approximate method of evaluating the influence of boundaries in order to apply existing aerodynamic data to hydrofoils and to correct properly data obtained in towing tanks to actual open-water conditions.

Experimental data at subcavitation speeds were obtained in two water depths at several depths of submergence at subcritical and supercritical speeds and are compared with aerodynamic data corrected for the boundary effects. The boundary-correction methods employed are similar to the general methods used in wind-tunnel research with the additional consideration that the limiting speed of wave propagation is taken into account.

SYMBOLS

A	geometric aspect ratio, $2s/c$
a_{0_1}	section lift-curve slope at infinite submergence, $dc_{l_1}/d\alpha_0$
a_{0_2}	section lift-curve slope at finite submergence, $dc_{l_2}/d\alpha_0$
a_1	slope of lift curve at infinite submergence, $dC_{L_1}/d\alpha$
a_2	slope of lift curve at finite submergence, $dC_{L_2}/d\alpha$
C_D	drag coefficient, D/qS
C_{D_i}	induced-drag coefficient of rectangular hydrofoil in infinite fluid
ΔC_{D_i}	induced-drag coefficient due to horseshoe-vortex images

[1] Supersedes recently declassified NACA RM L52D23a by Kenneth L. Wadlin, Charles L. Shuford, Jr., and John R. McGehee, 1952 and contains additional information from recently declassified NACA RM L51B13 by Kenneth L. Wadlin, Rudolph E. Fontana, and Charles L. Shuford, Jr., 1951.

δC_{D_t} induced-drag coefficient due to trailing-vortex images
C_{D_1} drag coefficient at infinite submergence, D_1/qS
C_{D_2} drag coefficient at finite submergence, D_2/qS
C_{D_3} wave-drag coefficient, D_3/qS
C_L lift coefficient, L/qS
C_{L_1} lift coefficient at infinite submergence, L_1/qS
C_{L_2} lift coefficient at finite submergence, L_2/qS
c chord of hydrofoil, ft
c_d section drag coefficient
c_{l_1} section lift coefficient at infinite submergence
c_{l_2} section lift coefficient at finite submergence
D drag, lb
D_1 drag at infinite submergence, lb
D_2 drag at finite submergence, lb
D_3 wave drag, lb
E_s effective-edge-velocity correction for lift
F Froude number based on depth of hydrofoil submergence, V^2/gf
f depth of quarter chord of hydrofoil below free-water surface, ft
g acceleration due to gravity, ft/sec^2
h depth of water, ft
L lift of hydrofoil, lb
L_1 lift at infinite submergence, lb
L_2 lift at finite submergence, lb
q free-stream dynamic pressure, $\frac{1}{2}\rho V^2$, lb/sq ft
R Reynolds number, Vc/ν
S area of hydrofoil, sq ft
s semispan of hydrofoil, ft
V free-stream velocity, ft/sec
V_c limiting speed of wave propagation or critical speed, ft/sec
W_1 induced vertical velocity at three-quarter chord due to bound vortex of hydrofoil (surface boundary only)
W_2 induced vertical velocity at three-quarter chord due to hydrofoil-image bound vortex (surface boundary only)
W_3 induced vertical velocity at three-quarter chord due to two trailing vortices of hydrofoil (surface boundary only)
W_4 induced vertical velocity at three-quarter chord due to two hydrofoil-image trailing vortices (surface boundary only)
W_5 induced vertical velocity at three-quarter chord due to horseshoe vortex of hydrofoil
W_6 induced vertical velocity at three-quarter chord due to hydrofoil-image horseshoe vortex (surface boundary only)
W_7 induced vertical velocity at three-quarter chord due to hydrofoil-image bound vortices (multiple boundaries)
W_8 induced vertical velocity at three-quarter chord due to hydrofoil-image trailing vortices (multiple boundaries)
x distance of bound vortex measured in free-stream direction from three-quarter chord of hydrofoil, ft
y distance to center of image horseshoe vortex, measured parallel to lifting line, from center of hydrofoil, ft
z distance of image bound vortex, measured normal to water surface, from hydrofoil quarter-chord point, ft
α angle of attack, deg
α_0 section angle of attack, deg
Γ circulation strength of vortex, $VcC_L/2$
Γ_1 circulation strength of vortex at infinite submergence
Γ_2 circulation strength of vortex at finite submergence
ν kinematic viscosity, ft^2/sec
ρ mass density, slugs/cu ft
σ plan-form correction factor for rectangular wings (see ref. 7)
ψ hydrofoil submergence parameter (see eq. (16))

DESCRIPTION OF MODELS

The experimental data were obtained by using 8-inch-chord hydrofoils with aspect ratios of 4 and 10, each supported by an 8-inch-chord strut intersecting the upper surface of the hydrofoil without fillets. The strut was perpendicular to the chord of the hydrofoil. The hydrofoil and struts were made of stainless steel and were polished to a smooth finish consistent with wind-tunnel practice.

The hydrofoils had an NACA 64_1A412 section which differs from the NACA 64_1–412 section only by elimination of the trailing-edge cusp; the section characteristics of these two are essentially the same (see ref. 1). The strut had an NACA 66_1–012 section. Table I (see page 22) gives the ordinates for the hydrofoil and strut sections as computed from references 1 and 2.

APPARATUS AND PROCEDURE

The tests on the aspect-ratio-10 hydrofoil were made in both Langley tank no. 1 and tank no. 2 to obtain two water depths. Figure 1 shows a view of the test setup with the aspect-ratio-10 hydrofoil and the balance attached to the structure on the Langley tank no. 2 carriage. The setup in Langley tank no. 1 was similar except for the method of attachment to the carriage. For the aspect-ratio-4 hydrofoil a sting support was used. Figure 2 shows a view of the test setup with the hydrofoil supporting sting and the balance attached to the structure of the Langley tank no. 2 carriage. The details of the supporting-sting arrangement are shown in figure 3. Figure 4 shows the cross sections of the two tanks. Tank no. 1 has a mean depth of 10.64 feet; tank no. 2 has a uniform depth of 6.0 feet.

The hydrofoils were moved vertically by means of a motor-driven jacking screw which moved the balance and hydrofoil as a unit. Change in angle of attack was obtained at the plate attaching the strut to the balance.

Measurements of lift and drag were made by means of electrical strain gages. The force measurements were made at constant speed, angle of attack, and depth of submergence. The depth of submergence is defined as the distance from the undisturbed water surface to the quarter-chord point on the chord line. For the aspect-ratio-10 hydrofoil, tests were

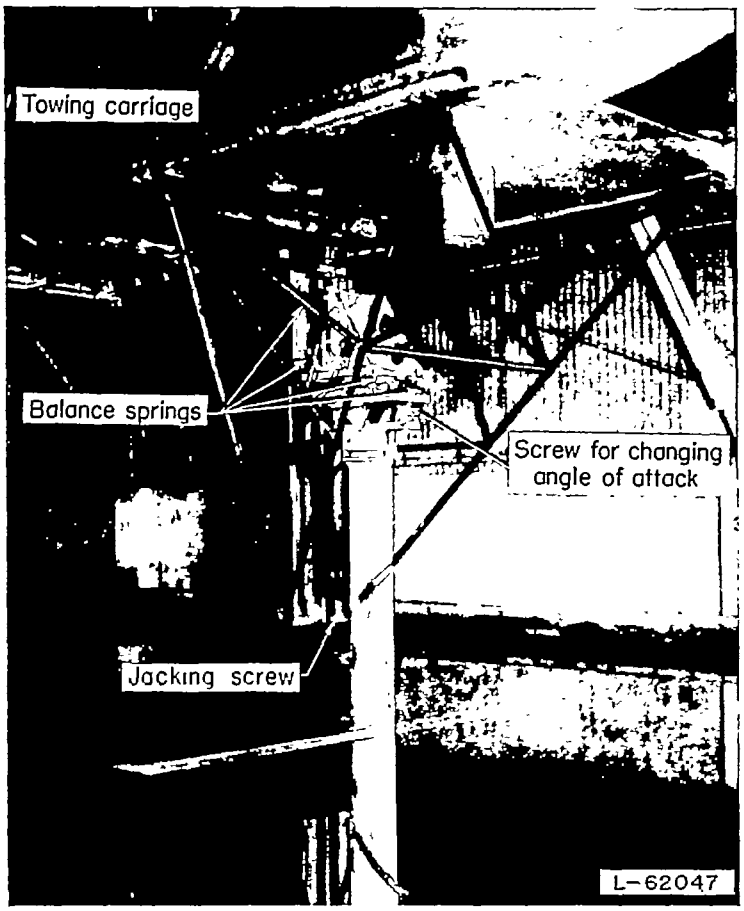

FIGURE 1.—Test setup showing aspect-ratio-10 hydrofoil and balance attached to towing carriage.

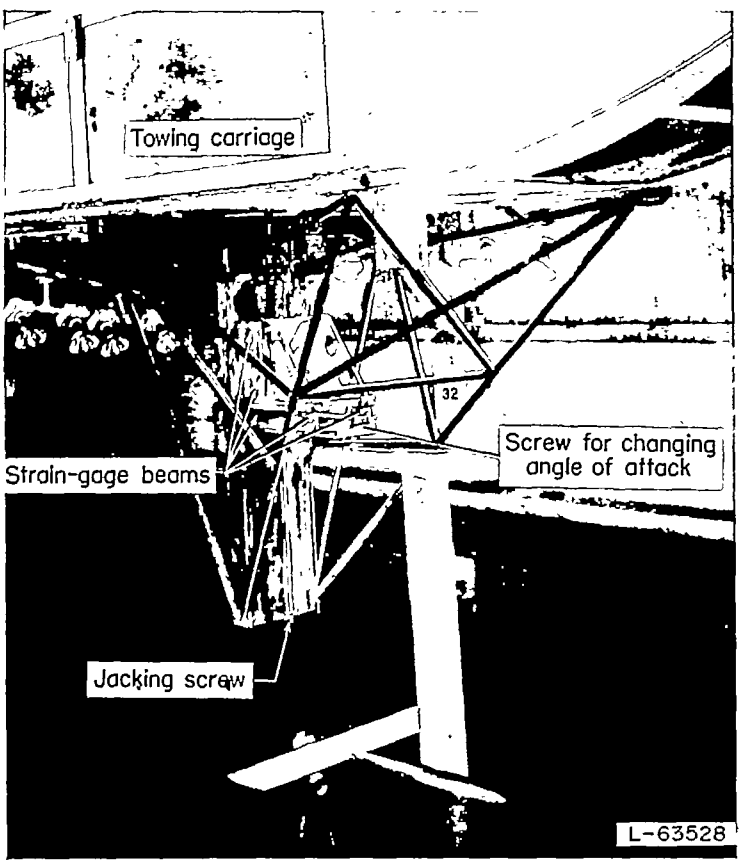

FIGURE 2.—Test setup showing aspect-ratio-4 hydrofoil suspended from balance attached to towing carriage.

413672—57——43

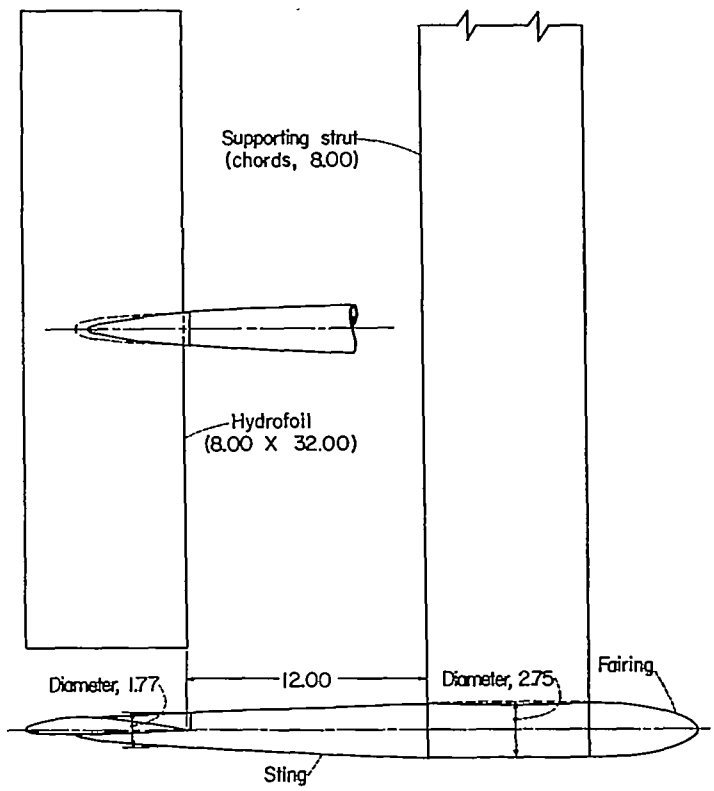

FIGURE 3.—Details of aspect-ratio-4 hydrofoil support arrangement. (All dimensions are in inches.)

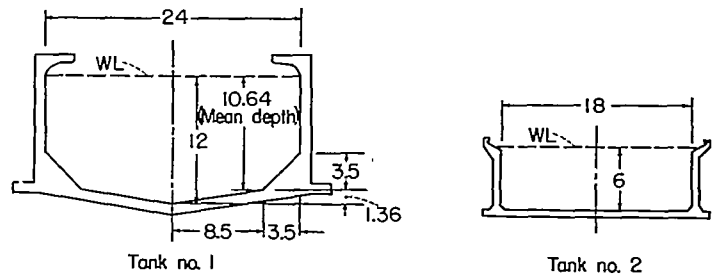

FIGURE 4.—Sectional details of Langley tanks no. 1 and no. 2. (All dimensions are in ft.)

made at two submergences (0.84 and 3.84 chords) over a range of speed from 5 to 45 fps and a range of angle of attack from −3.5° to 6.0°. For the aspect-ratio-4 hydrofoil, tests were made at five submergences (0.59, 1.09, 2.09, 3.09, and 4.09 chords) over a range of speed from 15 to 35 fps and a range of angle of attack from −3.5° to 4.0°. The change in angle of attack due to structural deflection caused by the lift and drag forces on the hydrofoil was obtained during the calibration of the balance, and the test data were adjusted accordingly.

The supporting strut for the aspect-ratio-10 hydrofoil and the supporting sting and strut for the aspect-ratio-4 hydrofoil were run alone at the same range of speed, depth, and angle of attack as when the hydrofoil was installed. For these tests the end of the strut (aspect-ratio-10 tare tests) and the end of the sting (aspect-ratio-4 tare tests) were fitted with faired caps. The tares thus obtained were deducted from the test data to give the net forces. The net forces were converted to the usual aerodynamic lift and drag coefficients by using a measured value of ρ of 1.966 slugs/cu ft

at the testing temperatures which were 40° F for the aspect-ratio-10 tests at 0.84 chord submergence in Langley tank no. 1, 44° F for all other tests with aspect-ratio-10 hydrofoil in both tanks, and 70° for tests with aspect ratio 4 in tank no. 2. All coefficients were based on the area of the hydrofoils. The area of the hydrofoils is 4.44 square feet for the aspect-ratio-10 hydrofoil and 1.78 square feet for the aspect-ratio-4 hydrofoil. The measured kinematic viscosity of the water at the time of the tests in tank no. 1 at 40° F was 1.85×10^{-5} ft²/sec, in tank no. 1 at 44° F was 1.73×10^{-5} ft²/sec, in tank no. 2 at 44° F was 1.83×10^{-5} ft²/sec, and in tank no. 2 at 70° F was 1.15×10^{-5} ft²/sec.

EXPERIMENTAL RESULTS

The basic experimental results corrected for strut deflection and drag tares are presented in figure 5 for the aspect-ratio-10 hydrofoil and in figure 6 for the aspect-ratio-4 hydrofoil as curves of lift and drag for each water depth and depth of hydrofoil submergence plotted against angle of attack with speed as the parameter. The data, converted to coefficients, are presented in figures 7 and 8 in the usual form for aerodynamic data. The strut drag coefficients (based on the area of the aspect-ratio-10 hydrofoil, 4.44 sq ft) plotted against speed in figure 9 indicate the range of strut drags obtained.

The lift-curve slopes and angles of zero lift obtained from figure 7 for the aspect-ratio-10 hydrofoil are plotted against Reynolds number in figure 10. Also included in this figure are the corresponding aerodynamic data for the NACA 65_3–418 section. These data were taken from reference 3 and the lift-curve slopes were corrected to aspect ratio 10 by the equation

$$a_1 = \frac{A a_{0_1}}{A E_e + \frac{57.3}{\pi} a_{0_1}} \tag{1}$$

from reference 4 where E_e is an effective-edge-velocity correction from reference 5. The hydrofoil data show no significant effect of tank depth at either depth of submergence. It is of particular interest to note that, where this effect would be expected to be most pronounced, namely, in the region between the dashed vertical lines of figure 10 where the speed in tank no. 1 is subcritical while that in tank no. 2 is supercritical, the lift-curve slope and the angle of zero lift for a given Reynolds number are essentially the same for both tanks. In the region below the critical speeds, the trends are not too apparent. The lift-curve slopes decrease and the angles of zero lift increase with decreasing Reynolds number, particularly at the shallower depth of submergence. Such a tendency is indicated by the corresponding low Reynolds number aerodynamic data for the NACA 65_3–418 section. The reason for the variation of this tendency with depth of submergence is not fully understood; however, changes in pressure distribution due to changes in submergence would influence the Reynolds number effect. It appears therefore that, if the lift-curve slopes and angles of zero lift are influenced by the critical speed, the influence indicated by these tests is so small as to be masked by Reynolds number effects encountered in the tests and by the effects of submergence.

The variation of drag coefficient with speed for the 10.64-foot and the 6.0-foot water depths at lift coefficients of 0.4 and 0.6 and depths of submergence of 0.84 and 3.84 chords and aerodynamic section drag data at the same lift coefficients for the NACA 65_3–418 airfoil section from reference 3 are shown in figure 11. A comparison of the drag coefficients for the two water depths at both lift coefficients and both depths of submergence shows that, with reducing speed, when the critical speed in the greater water depth (tank no. 1, 15.98 chords) was approached, a drag rise occurred whereas the drag in the shallower water depth (tank no. 2, 9 chords) did not rise until its lower critical speed was approached. It can be seen that the drag rise increases with lift coefficient and decreases with depth of submergence. The variation in drag rise with lift coefficient and depth of submergence is as predicted by the theory that will be discussed subsequently. However, the drag rise was gradual rather than the abrupt rise predicted by this theory. The trends at the low subcritical speeds are not too clear since they are masked by Reynolds number effects. An indication of the possible Reynolds number effects can be obtained from the aerodynamic data presented.

THEORETICAL BOUNDARY CORRECTIONS—SUPERCRITICAL

GENERAL

In order to use aerodynamic data for an airfoil in an infinite medium to predict the characteristics of a hydrofoil in the proximity of the water surface and perhaps rigid boundaries as would be encountered in shallow water, canals, or towing tanks, the influence of these boundaries must be evaluated. The boundary condition to be satisfied at the free surface is that of constant pressure along the surface streamlines. The boundary condition to be satisfied at the rigid boundaries is zero normal velocity.

FREE-SURFACE BOUNDARY

As a first approximation to the three-dimensional problem supercritical conditions are assumed, however, with only the free-water-surface boundary present. The constant-pressure boundary at the free surface can be satisfied by the introduction of a horseshoe vortex above the surface which has the same direction of rotation as the one which represents the loading on the hydrofoil (fig. 12).

The presence of the image bound vortex does not change the direction of the flow relative to the hydrofoil chord line in the vicinity of the center of pressure, but it does tend to curve the streamlines relative to the hydrofoil chord line. The curvature effect is equivalent to introducing camber of the hydrofoil in such a manner as to produce a negative lift increment. It would seem therefore that a reasonably close approximation to the effect of the free surface could be obtained by simply evaluating the effect of streamline curvature, in addition to the induced-angle effect of the trailing vortices, by applying a technique frequently used in approximate solutions of aerodynamic problems (see ref. 6). This technique involves determination of the circulation Γ required to produce a downward velocity $W_5 + W_6$ at the

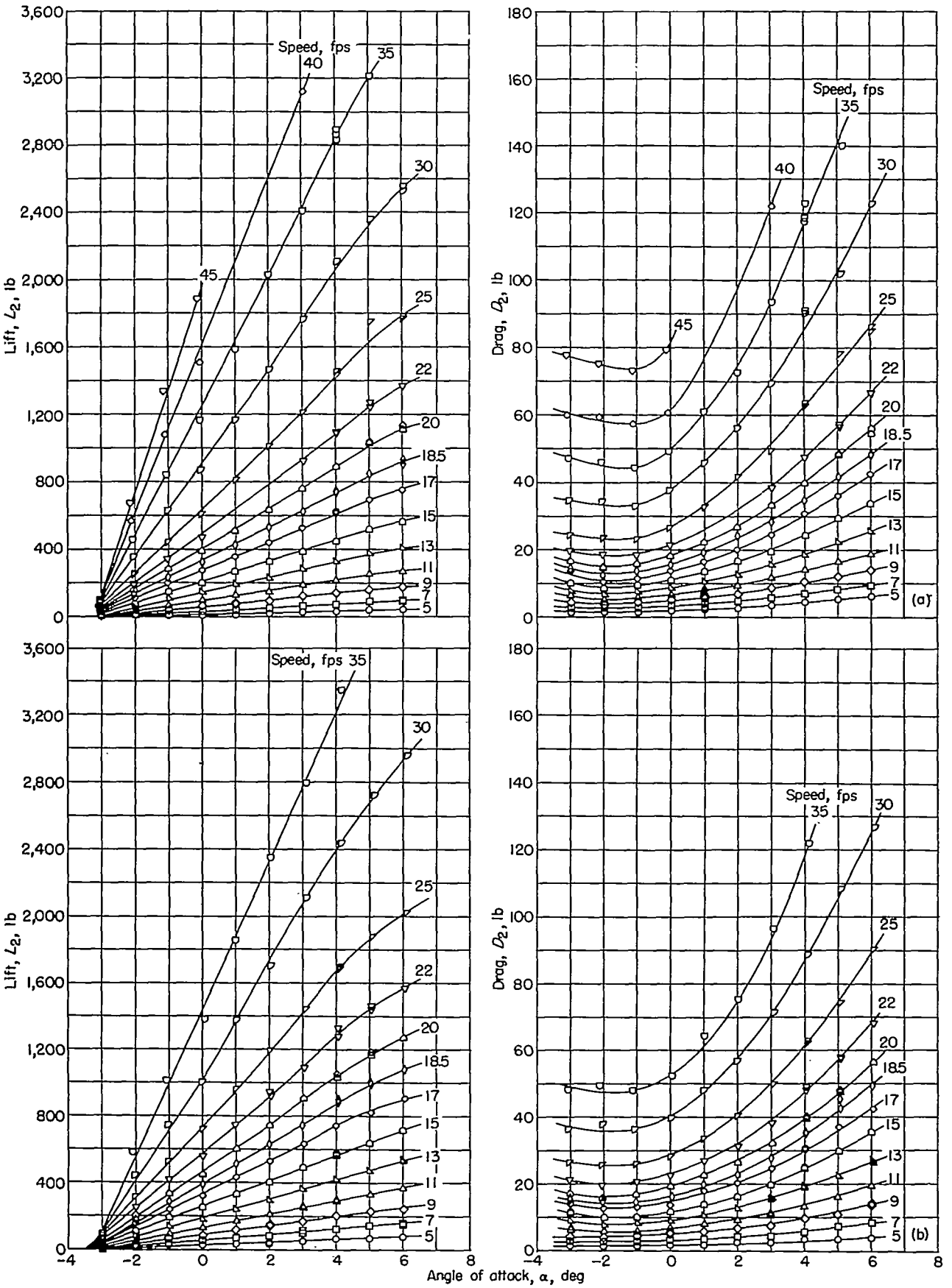

(a) Water depth, 10.64 feet (15.98 chords); depth of submergence, 0.84 chord.
(b) Water depth, 10.64 feet (15.98 chords); depth of submergence, 3.84 chords.

FIGURE 5.—Lift and drag of the aspect-ratio-10 hydrofoil.

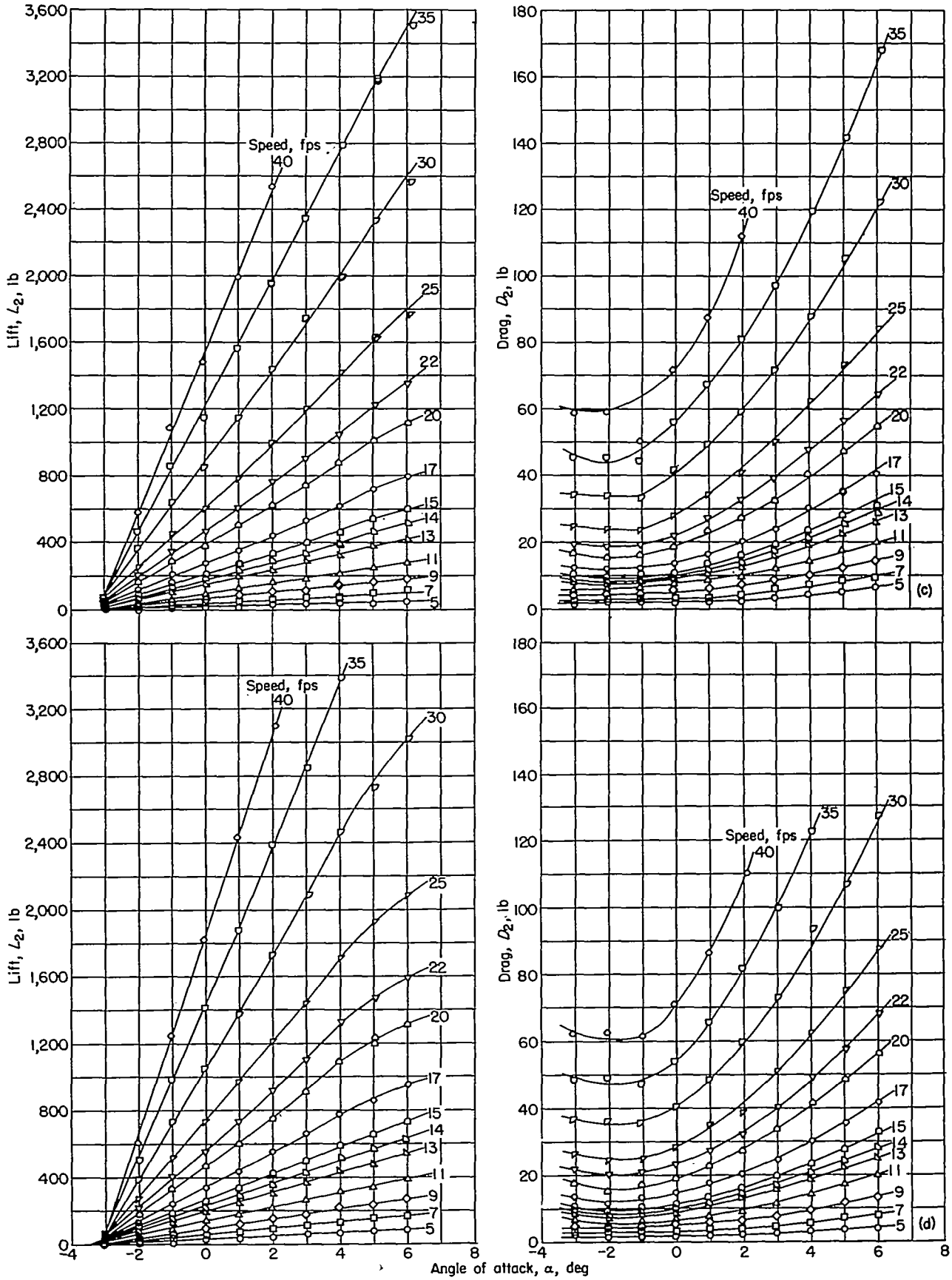

(c) Water depth, 6.0 feet (9.0 chords); depth of submergence, 0.84 chord.
(d) Water depth, 6.0 feet (9.0 chords); depth of submergence, 3.84 chords.

FIGURE 5.—Concluded.

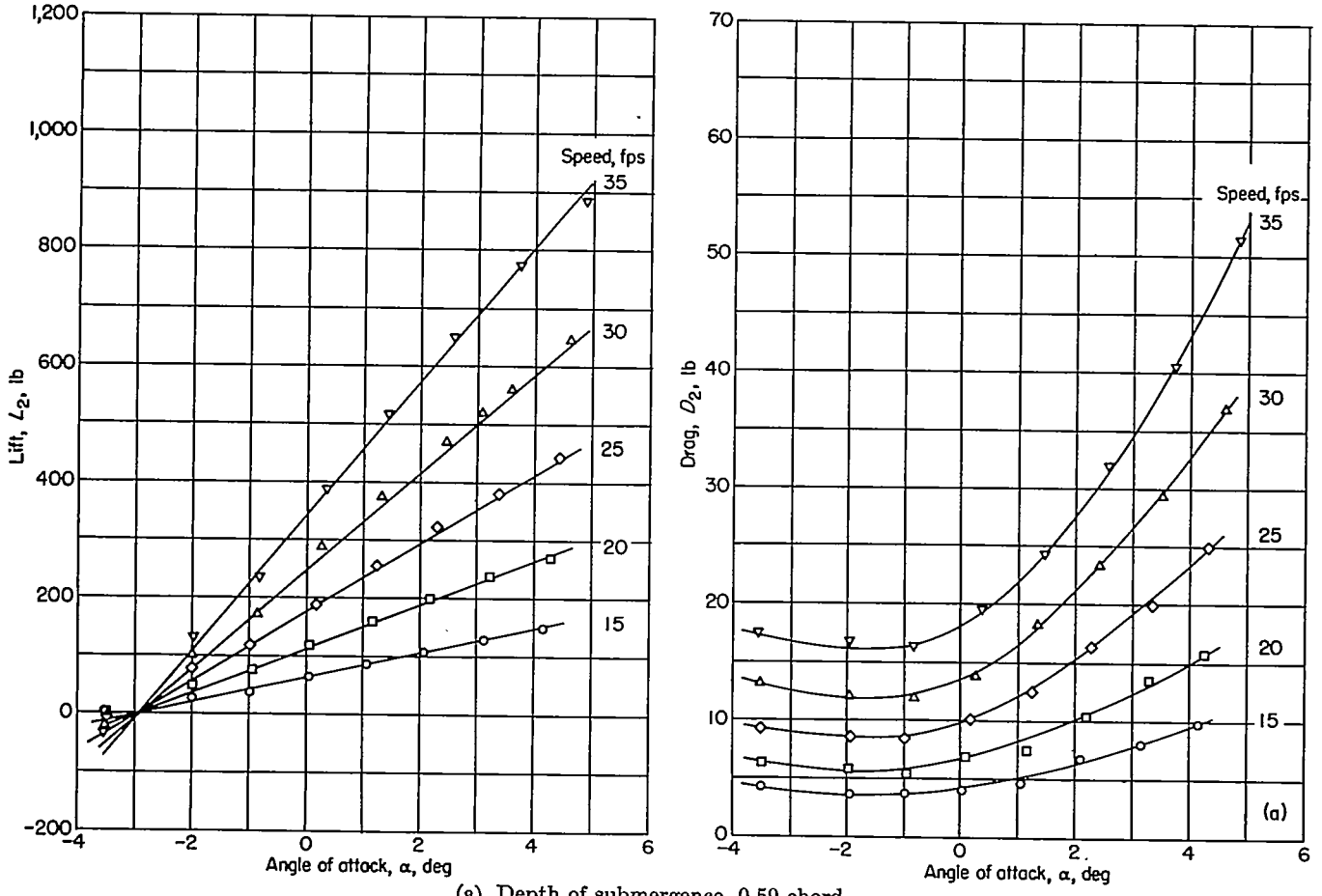

(a) Depth of submergence, 0.59 chord.

FIGURE 6.—Lift and drag of the aspect-ratio-4 hydrofoil. Water depth, 6.0 feet (9.0 chords).

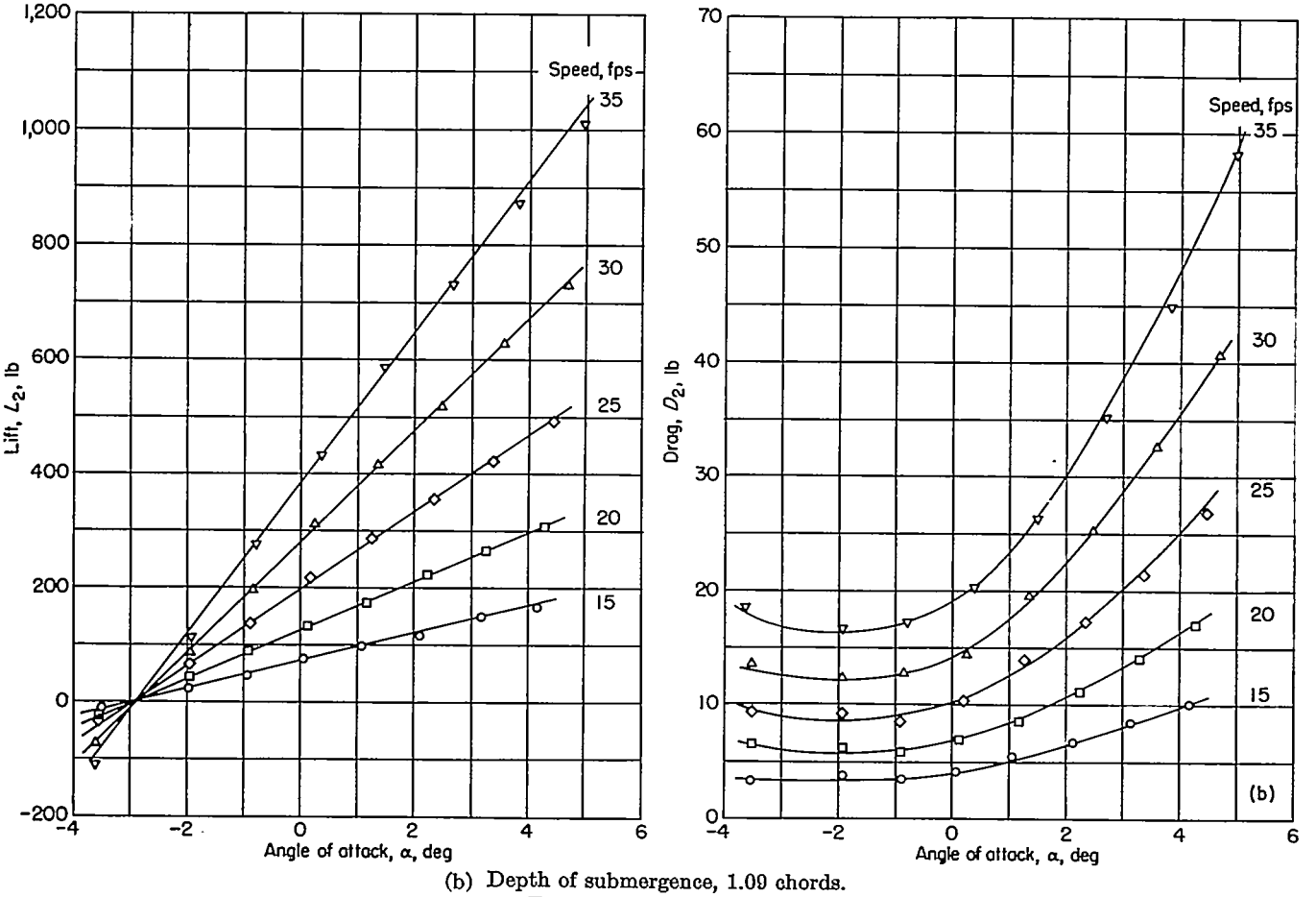

(b) Depth of submergence, 1.09 chords.

FIGURE 6.—Continued.

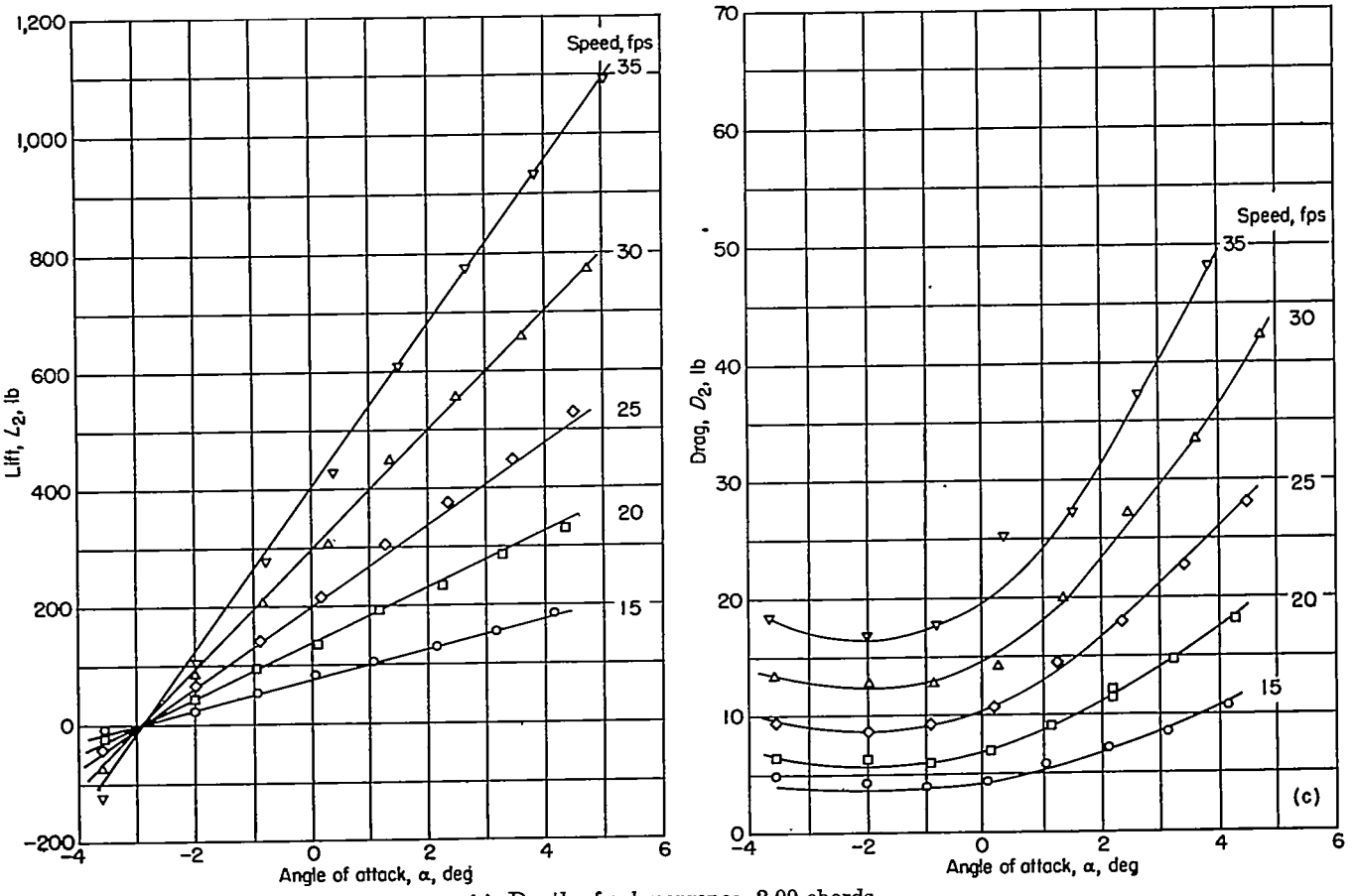

(c) Depth of submergence, 2.09 chords.

FIGURE 6.—Continued.

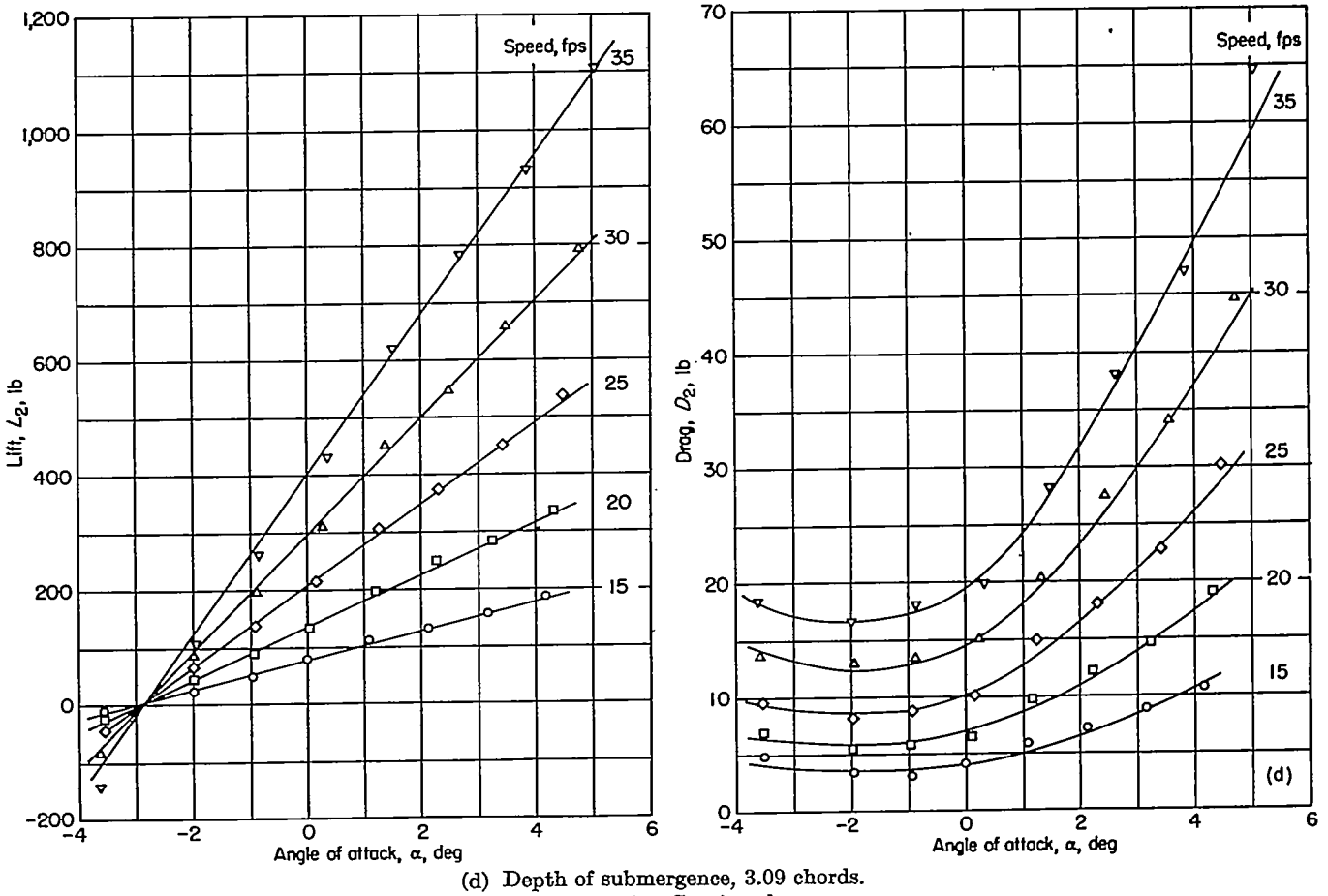

(d) Depth of submergence, 3.09 chords.

FIGURE 6.—Continued.

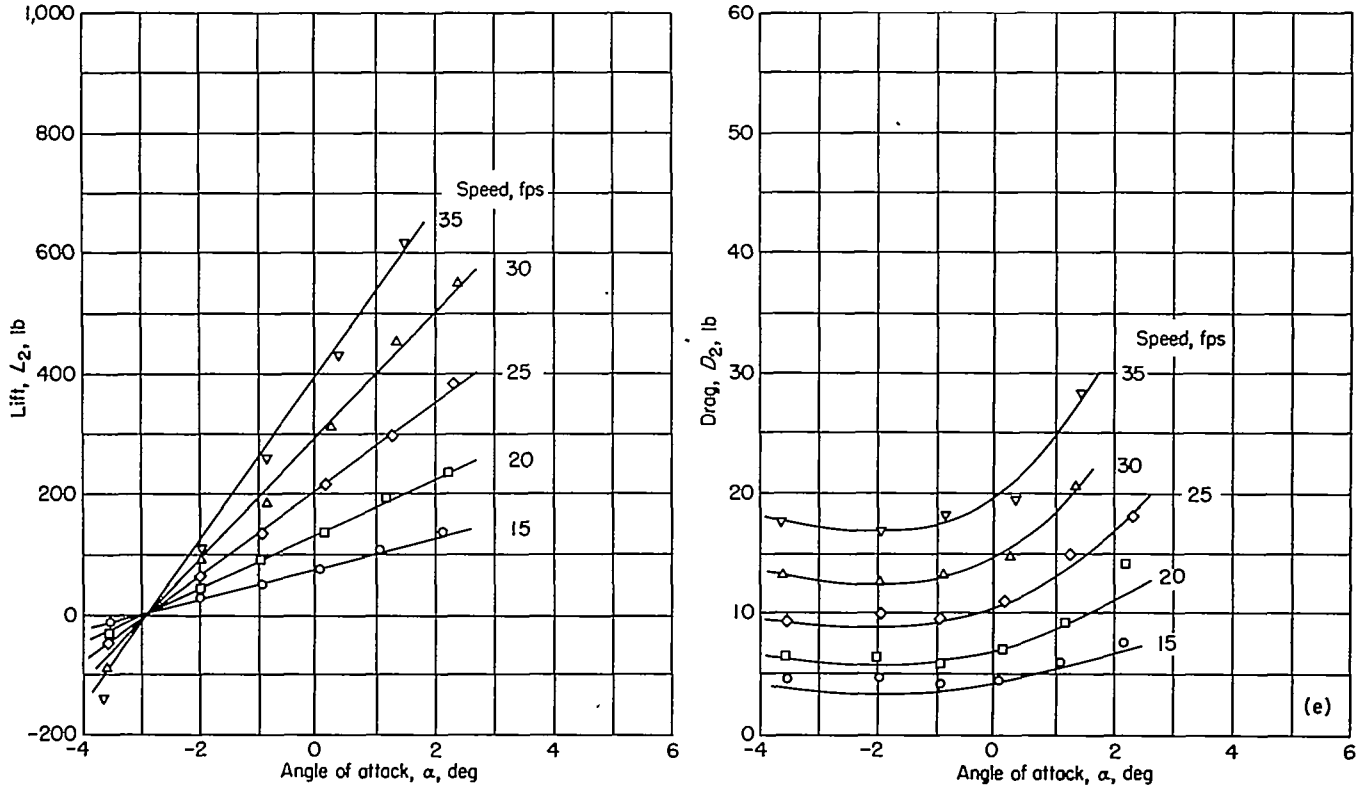

(e) Depth of submergence, 4.09 chords.

FIGURE 6.—Concluded.

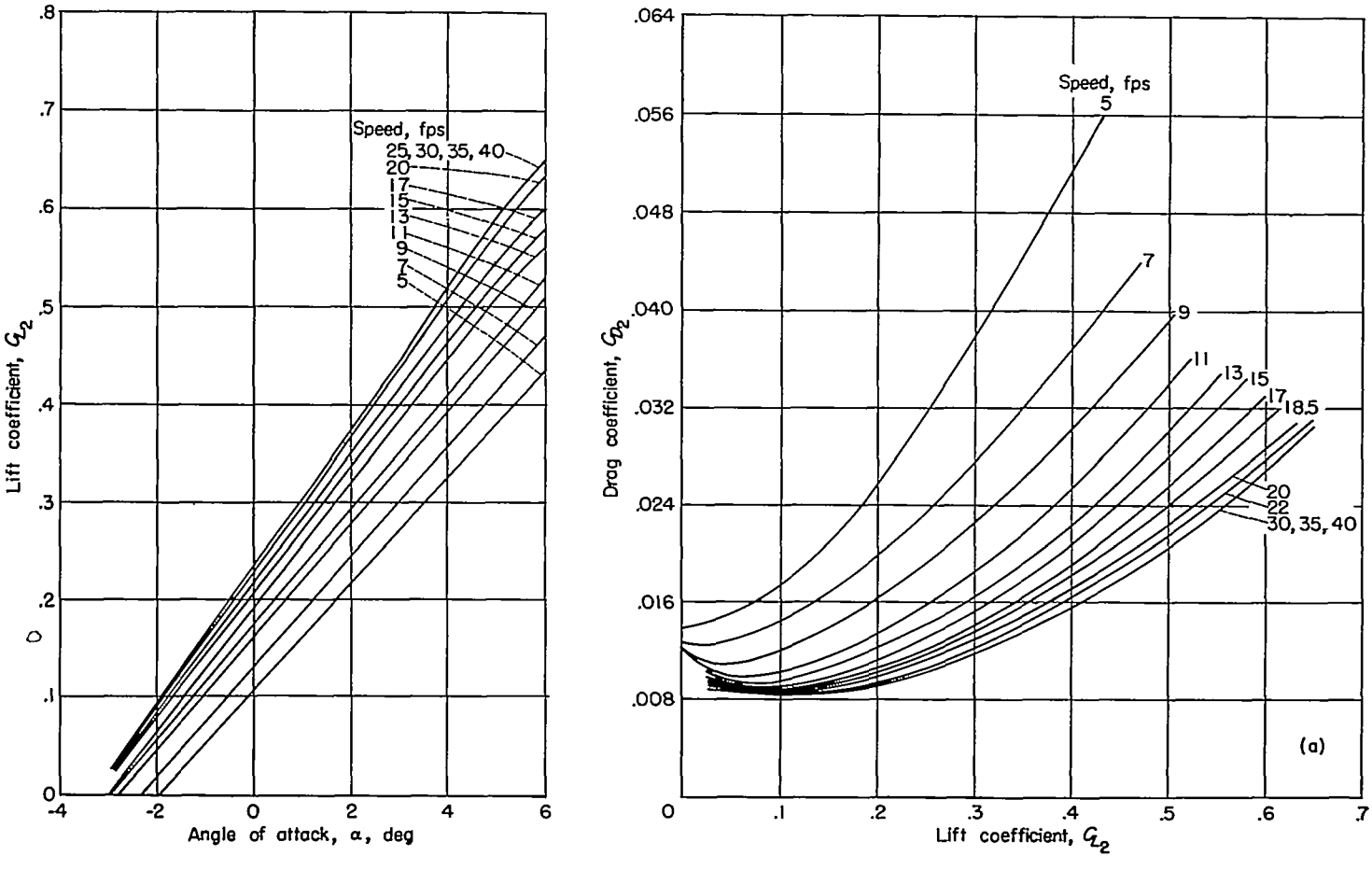

(a) Water depth, 10.64 feet (15.98 chords); depth of submergence, 0.84 chord.

FIGURE 7.—Lift and drag coefficients of the aspect-ratio-10 hydrofoil.

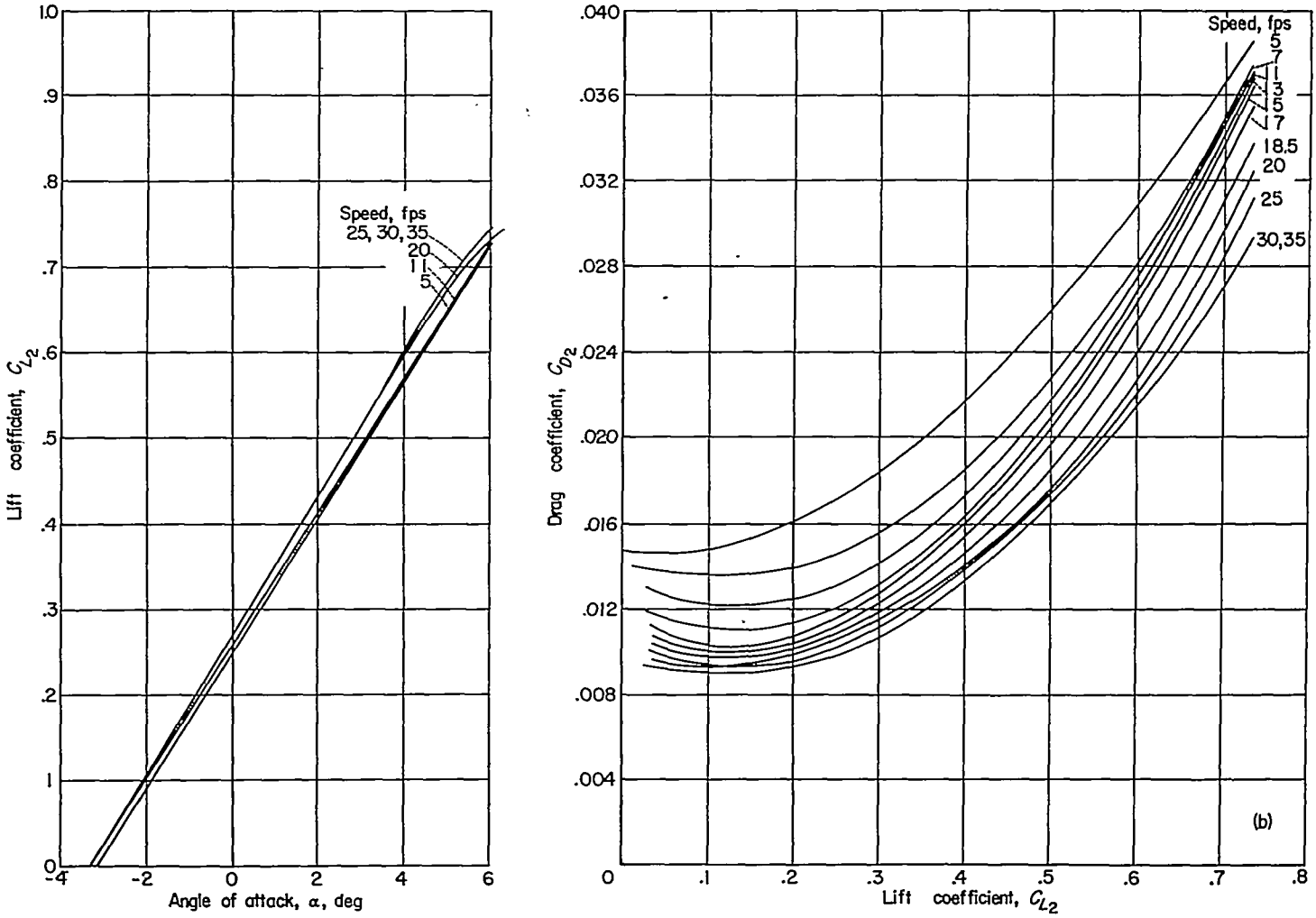

(b) Water depth, 10.64 feet (15.98 chords); depth of submergence, 3.84 chords.

FIGURE 7.—Continued.

three-quarter-chord location which when combined with the free-stream velocity V produces a flow tangent to the mean camber line of the hydrofoil. Thus, if geometric camber is neglected, the hydrofoil angle of attack α is equal to the sum of the angles at the three-quarter-chord point induced by the hydrofoil vortices and their images located at a distance directly above the hydrofoil equal to twice the depth of submergence.

By use of the Biot-Savart law and the notations defined in figure 12, the following expressions for the separate contributions at the line of symmetry to the vertical component of the induced velocity at the three-quarter chord were obtained:

The contribution due to the bound vortex of the hydrofoil,

$$W_1=\frac{\Gamma}{\pi c}\frac{s}{\sqrt{\left(\frac{c}{2}\right)^2+s^2}} \tag{2}$$

the contribution due to the image bound vortex,

$$W_2=\frac{\Gamma}{4\pi\left[\left(\frac{c}{2}\right)^2+(2f)^2\right]}\frac{sc}{\sqrt{\left(\frac{c}{2}\right)^2+(2f)^2+s^2}} \tag{3}$$

the contribution due to the two trailing vortices of the hydrofoil,

$$W_3=\frac{\Gamma}{2\pi s}\left[\frac{c}{2\sqrt{\left(\frac{c}{2}\right)^2+s^2}}+1\right] \tag{4}$$

the contribution due to the two image trailing vortices,

$$W_4=\frac{\Gamma s}{2\pi[s^2+(2f)^2]}\left[\frac{c}{2\sqrt{\left(\frac{c}{2}\right)^2+s^2+(2f)^2}}+1\right] \tag{5}$$

the contribution due to the horseshoe vortex of the hydrofoil,

$$W_5=\frac{\Gamma}{2\pi}\left[\frac{2}{sc}\sqrt{\left(\frac{c}{2}\right)^2+s^2}+\frac{1}{s}\right] \tag{6}$$

and the contribution due to the image horseshoe vortex

$$W_6=\frac{\Gamma}{4\pi}\left\{\frac{c}{\left(\frac{c}{2}\right)^2+(2f)^2}\frac{s}{\sqrt{\left(\frac{c}{2}\right)^2+(2f)^2+s^2}}+\frac{2s}{(2f)^2+s^2}\left[1+\frac{c}{2\sqrt{\left(\frac{c}{2}\right)^2+(2f)^2+s^2}}\right]\right\} \tag{7}$$

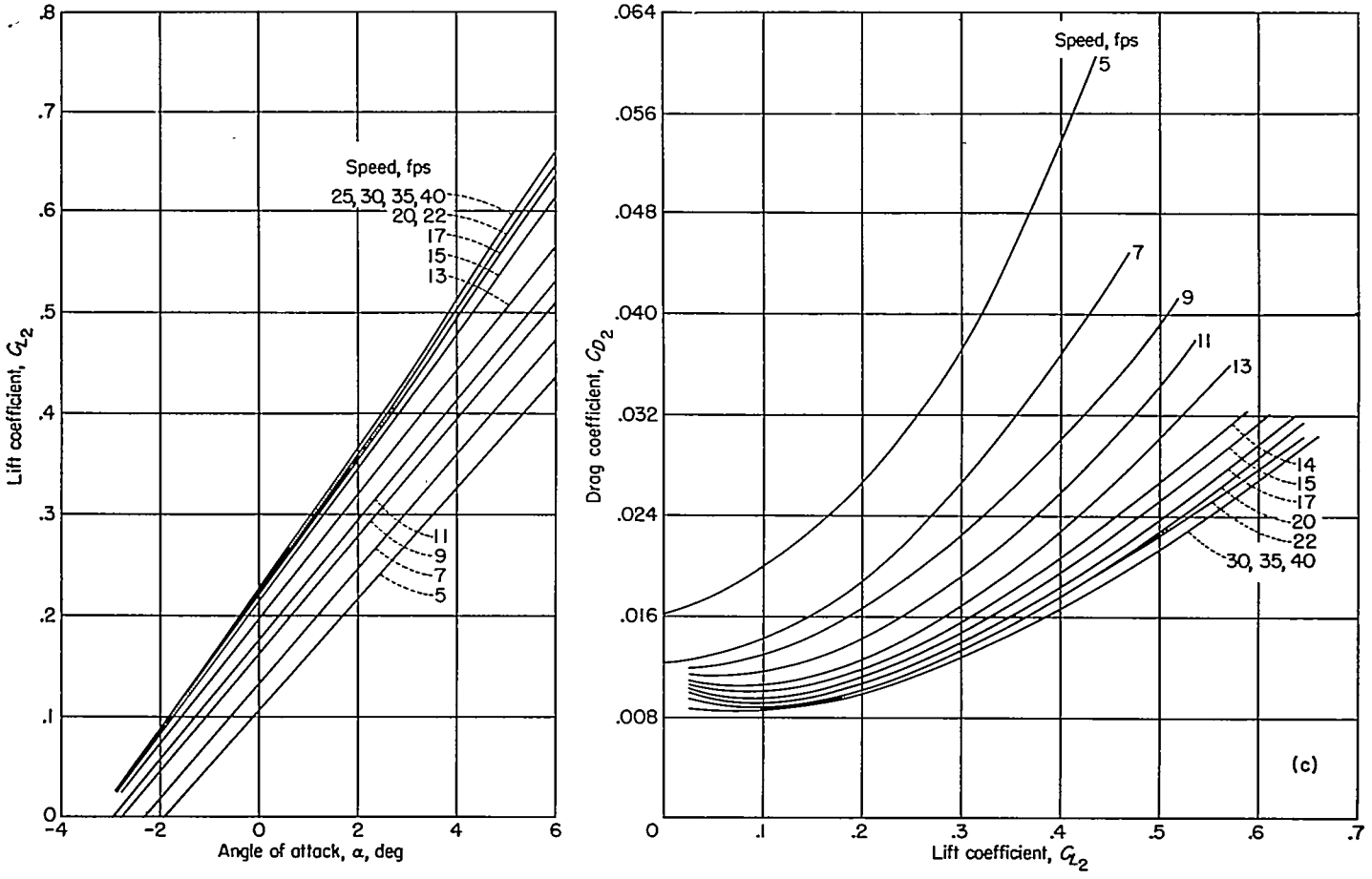

(c) Water depth, 6.0 feet (9.0 chords); depth of submergence, 0.84 chord.

FIGURE 7.—Continued

By means of equations (6) and (7) a computation of the angle of attack α can be made.

Effect on lift.—In order to estimate the effect of depth of submergence on lift, the ratio of the hydrofoil circulation in an infinite fluid to that of a hydrofoil at a finite depth of submergence for a given angle of attack is obtained; that is,

$$\frac{\Gamma_1}{\Gamma_2}=\frac{W_5+W_6}{W_5}=1+\frac{W_6}{W_5} \tag{8}$$

Therefore (for small angles),

$$\frac{\Gamma_1}{\Gamma_2}=1+\frac{\dfrac{sc}{2\sqrt{\left(\frac{c}{2}\right)^2+(2f)^2+s^2}}\left[\dfrac{1}{\left(\frac{c}{2}\right)^2+(2f)^2}+\dfrac{1}{(2f)^2+s^2}\right]+\dfrac{s}{(2f)^2+s^2}}{\dfrac{2}{sc}\sqrt{s^2+\left(\frac{c}{2}\right)^2}+\dfrac{1}{s}}$$

where

$$\Gamma=\frac{VcC_L}{2}$$

and

$$\frac{\Gamma_2}{\Gamma_1}=\frac{C_{L_2}}{C_{L_1}}=\frac{a_2}{a_1}$$

Rewriting this equation to get f in terms of c and substituting

$$A=\frac{2s}{c}$$

yields

$$\frac{a_2}{a_1}=\frac{1}{1+\dfrac{\dfrac{A}{4\sqrt{\frac{1}{4}+4\left(\frac{f}{c}\right)^2+\frac{A^2}{4}}}\left[\dfrac{1}{\frac{1}{4}+4\left(\frac{f}{c}\right)^2}+\dfrac{1}{\frac{A^2}{4}+4\left(\frac{f}{c}\right)^2}\right]+\dfrac{1}{\frac{8}{A}\left(\frac{f}{c}\right)^2+\frac{A}{2}}}{\frac{2}{A}\left(\sqrt{A^2+1}+1\right)}} \tag{9}$$

which is the ratio of lift-curve slope at finite depth to that at infinite depth when only the free surface is considered.

For the two-dimensional case, only the induced velocities due to the bound vortex W_1 and the image bound vortex W_2 are considered in equation (8); thus,

$$\frac{a_{0_2}}{a_{0_1}}=\frac{\left(4\frac{f}{c}\right)^2+1}{\left(4\frac{f}{c}\right)^2+2}$$

which is the ratio of the two-dimensional lift-curve slope at finite depth to that at infinite depth when only the free surface is considered.

Effect on drag.—In order to estimate the effect of depth of submergence on the drag of a finite-span rectangular

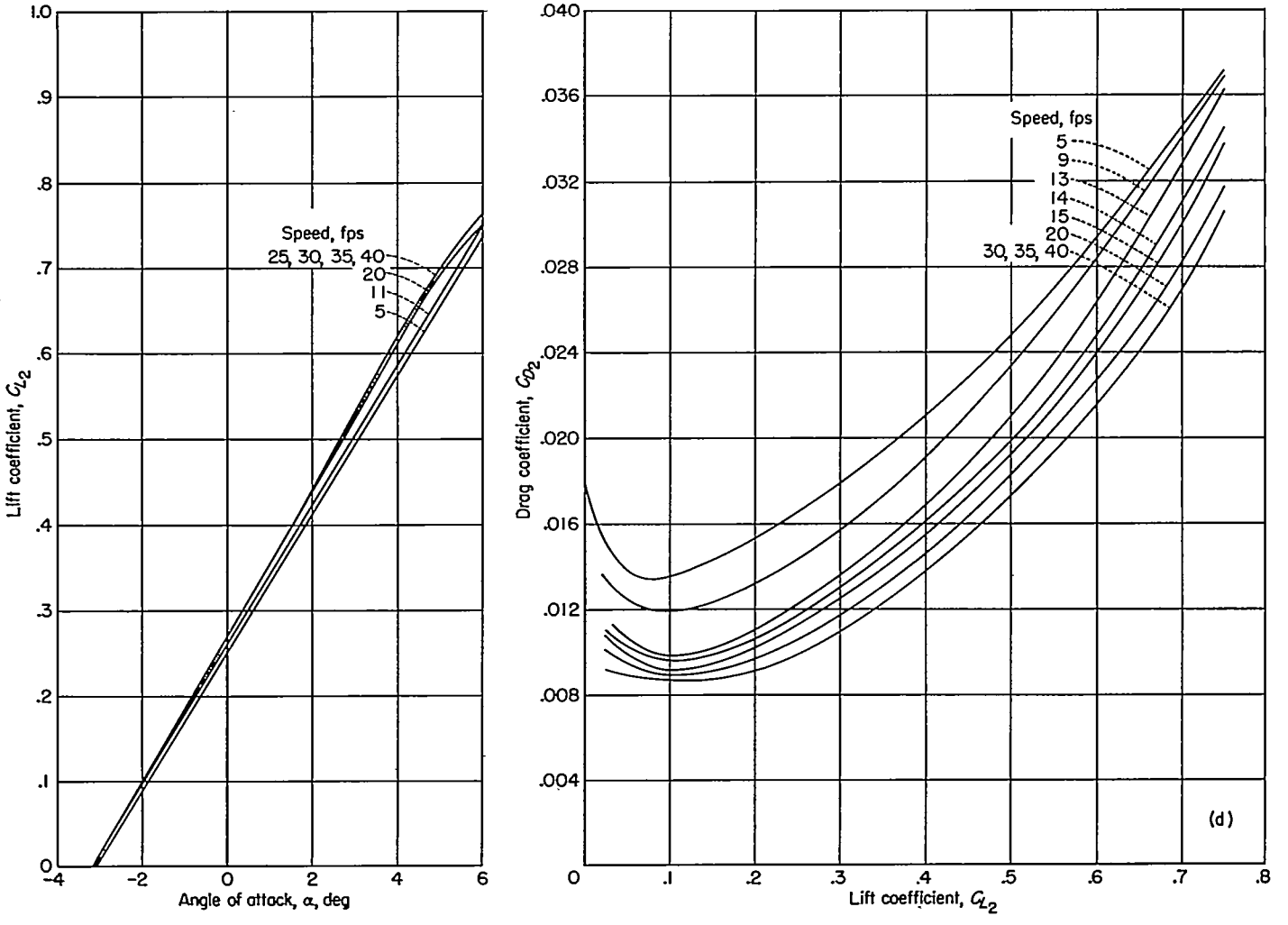

(d) Water depth, 6.0 feet (9.0 chords); depth of submergence, 3.84 chords.

FIGURE 7.—Concluded.

hydrofoil, the drag induced by the hydrofoil images at a given angle of attack is obtained from the equation

$$\Delta C_{D_i}=C_{L_2}\frac{W_s}{V}(1+\sigma) \tag{10}$$

This relation is not rigorous since it gives an induced drag in two-dimensional flow due to the influence of the bound vortex at the three-quarter chord. However, for the aspect ratios under consideration, when the drag correction is determined in the usual manner, that is by evaluating the downwash at the quarter chord, the drag predicted is too low. This condition is true even when the spanwise distribution of downwash is considered.

From equation (7)

$$\frac{W_s}{V}=\frac{\Gamma}{4\pi V}K$$

where

$$K=\frac{c}{\left(\frac{c}{2}\right)^2+4f^2}\left[\frac{s}{\sqrt{\left(\frac{c}{2}\right)^2+4f^2+s^2}}+\frac{2s}{4f^2+s^2}\left(1+\frac{c}{2\sqrt{\left(\frac{c}{2}\right)^2+4f^2+s^2}}\right)\right]$$

The drag coefficient of a rectangular hydrofoil in an infinite fluid is

$$C_{D_1}=c_d+\frac{C_{L_1}^2}{\pi A}(1+\sigma)$$

The total drag coefficient of a rectangular hydrofoil at a given depth of submergence and angle of attack, therefore, is

$$C_{D_2}=c_d+C_{L_2}\left(\frac{1}{A\pi}+\frac{Kc}{8\pi}\right)(1+\sigma) \tag{11}$$

RESTRICTED AREA

In order to estimate the effect of depth of submergence on the lift and drag of a hydrofoil in a restricted area such as a shallow harbor, a canal, or a towing tank, a system of images (fig. 13) that satisfied the boundary conditions of constant pressure at the free-water surface and zero normal velocity at the rigid boundaries is required. The boundary-induced vertical velocities at the three-quarter chord are obtained by computing the combined effect of sufficient images to give the desired accuracy. An infinite array of images is, of course, required to give an exact value.

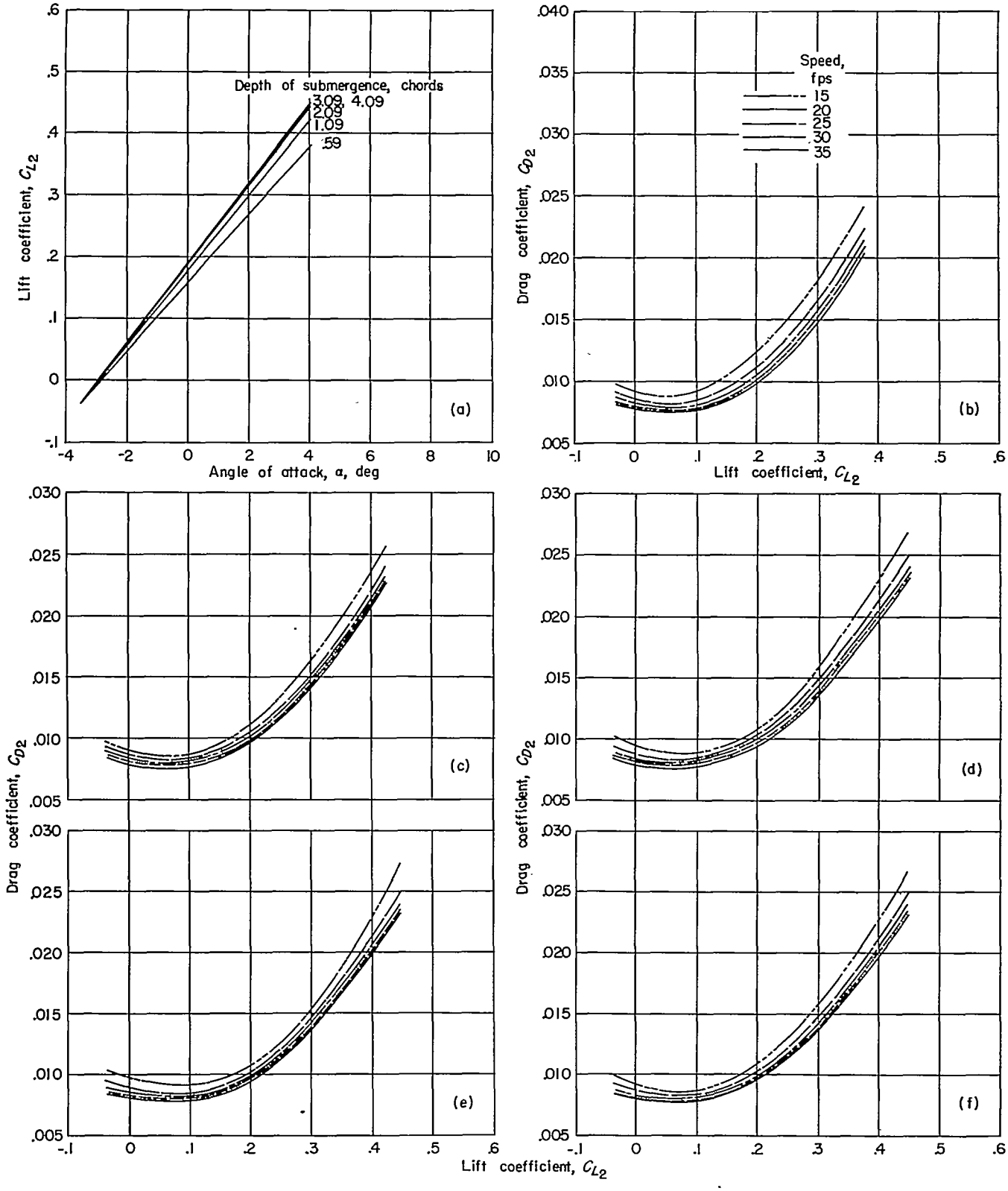

(a) Lift at all speeds.
(b) Drag; depth of submergence, 0.59 chord.
(c) Drag; depth of submergence, 1.09 chords.
(d) Drag; depth of submergence, 2.09 chords.
(e) Drag; depth of submergence, 3.09 chords.
(f) Drag; depth of submergence, 4.09 chords.

FIGURE 8.—Lift and drag coefficients of the aspect-ratio-4 hydrofoil.

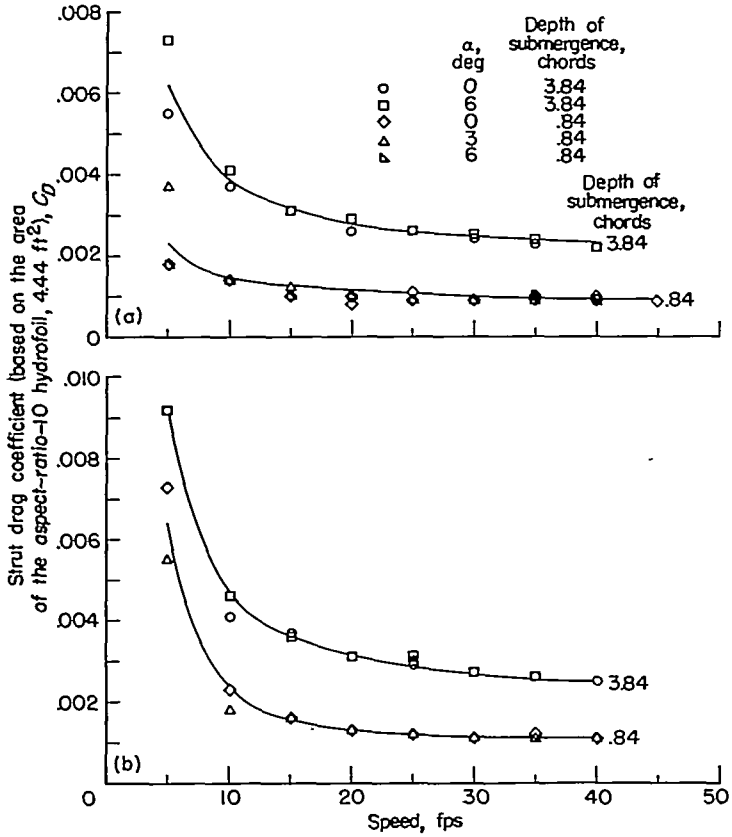

(a) Tank no. 1.
(b) Tank no. 2.

FIGURE 9.—Variation of strut drag coefficient with speed and depth of hydrofoil submergence for the aspect-ratio-10 hydrofoil.

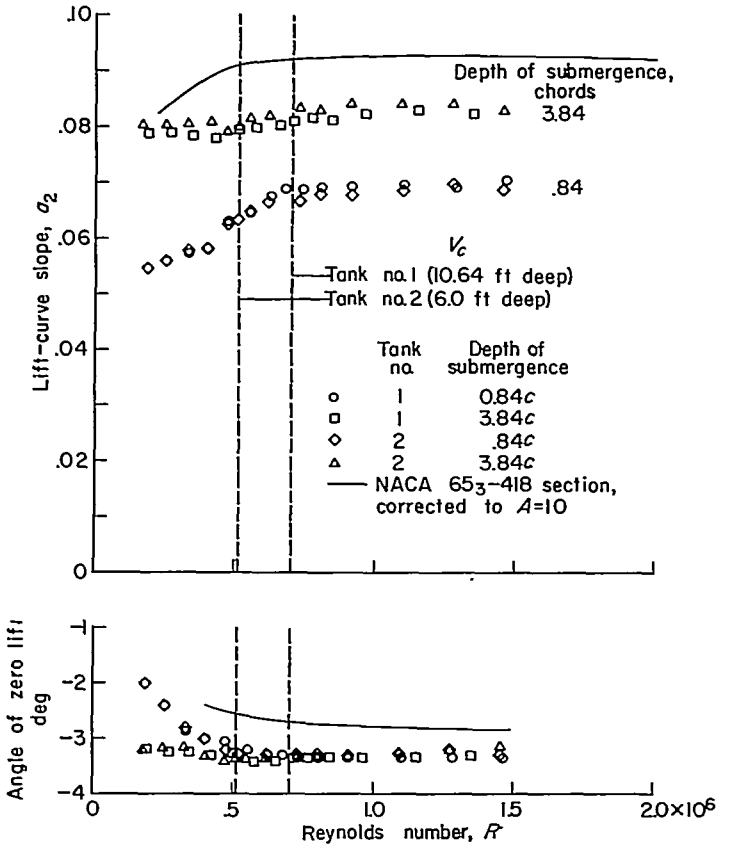

FIGURE 10.—Variation of lift-curve slope and angle of zero lift with Reynolds number for the aspect-ratio-10 hydrofoil.

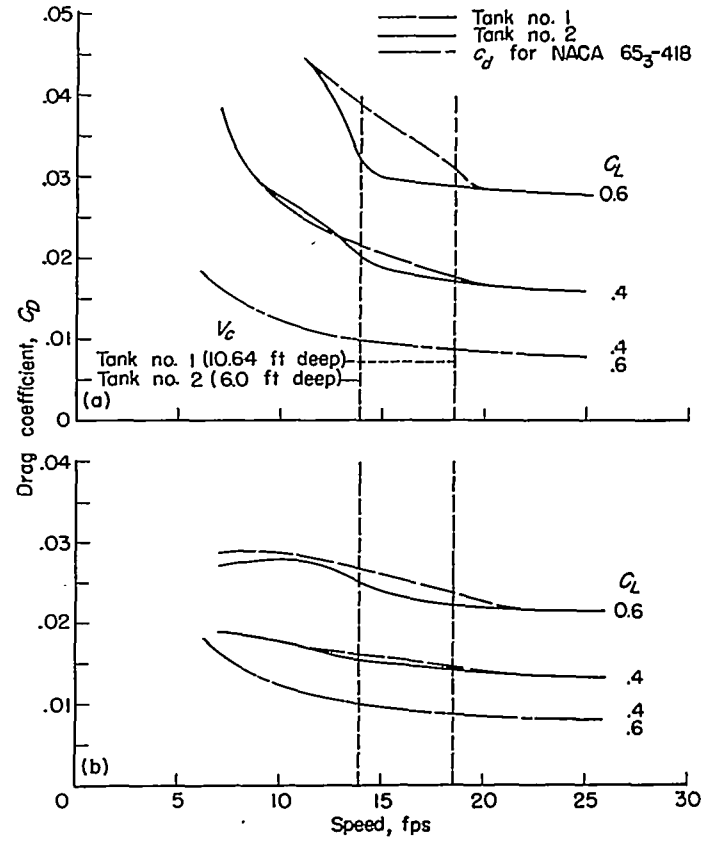

(a) Depth of submergence, 0.84 chord.
(b) Depth of submergence, 3.84 chords.

FIGURE 11.—Variation of drag coefficient of aspect-ratio-10 hydrofoil with speed for constant lift coefficient.

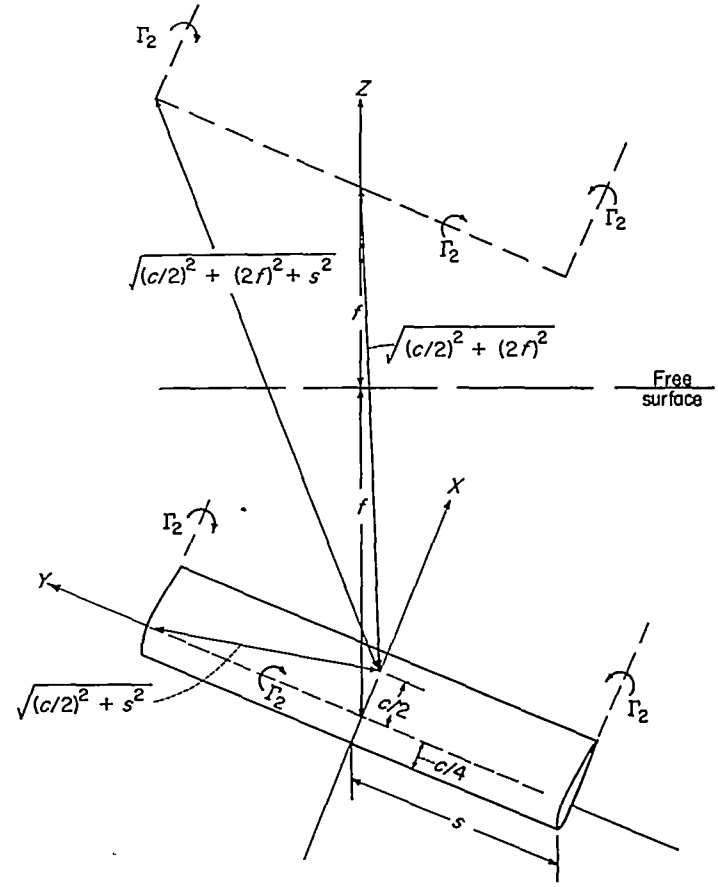

FIGURE 12.—Horseshoe-vortex arrangement that satisfies the free-surface boundary.

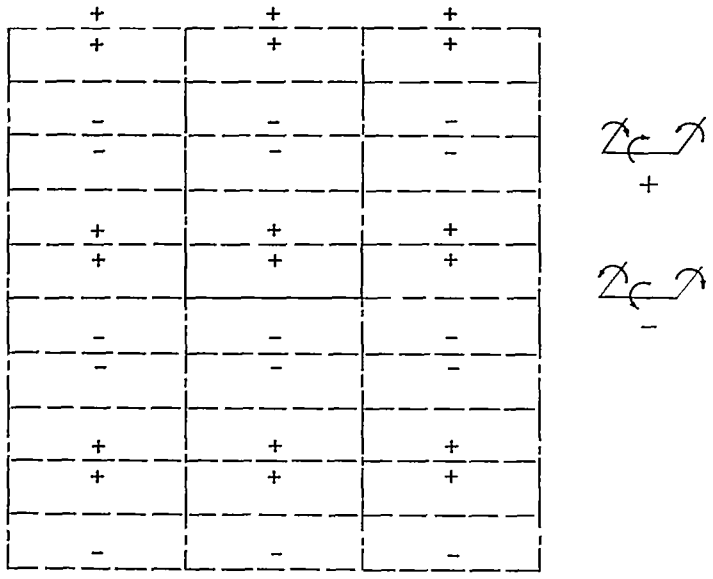

FIGURE 13.—Horseshoe-vortex arrangement that satisfactorily approximates the tank boundary conditions.

Sufficient accuracy, however, can be obtained with a finite array of images. For example, if another row of images were added to the top and bottom and another column of images to each side of the horseshoe vortex arrangement shown in figure 13 (A=10, tank no. 2, submergence of 0.84 chord) the additional images would cause a change of less than 1 percent in the total induced vertical velocity at the three-quarter chord of the hydrofoil. The general equation for this velocity for each image vortex (see ref. 7) is:

For the image bound vortex

$$W_7=\frac{\Gamma}{4\pi}\frac{x}{x^2+z^2}\left[\frac{y+s}{\sqrt{x^2+z^2+(y+s)^2}}-\frac{y-s}{\sqrt{x^2+z^2+(y-s)^2}}\right] \quad (12)$$

and for two image trailing vortices

$$W_8=\frac{\Gamma}{4\pi}\left\{\frac{y+s}{z^2+(y+s)^2}\left[1+\frac{x}{\sqrt{x^2+z^2+(y+s)^2}}\right]-\frac{y-s}{z^2+(y-s)^2}\left[1+\frac{x}{\sqrt{x^2+z^2+(y-s)^2}}\right]\right\} \quad (13)$$

where x, y, and z define the location of the image with respect to the intersection of the quarter-chord line and the line of symmetry of the hydrofoil (see fig. 12).

The ratio a_2/a_1 and the drag coefficient C_D are obtained as previously discussed by substituting W_7+W_8 for W_6 in equations (8) and (10).

Some results calculated by applying the foregoing theoretical method in tanks no. 1 and no. 2 for estimating the effect of submergence on lift-curve slope are shown in figure 14 for three aspect ratios.

COMPARISON OF THEORY AND EXPERIMENT

Lift.—The theoretical results presented in figure 14 are compared in figure 15 with the present experimental results for hydrofoils of aspect ratios 4 and 10 and with experimental results given in references 8 and 9 for hydrofoils of aspect ratios 10 and 6, respectively. The ratio a_2/a_1 for the experimental lift-curve slopes for hydrofoils of aspect ratios 6 and 10 is the ratio of the lift-curve slope obtained at a given depth of submergence to the lift-curve slope (corrected for aspect ratio by eq. (1)) as obtained for airfoil data (see refs. 10 and 11). The ratio a_2/a_1 for the experimental lift-curve slopes for the aspect-ratio-4 hydrofoil is the ratio of the lift-curve slope obtained at a given depth of submergence to the lift-curve slope at the greatest depth of submergence. This

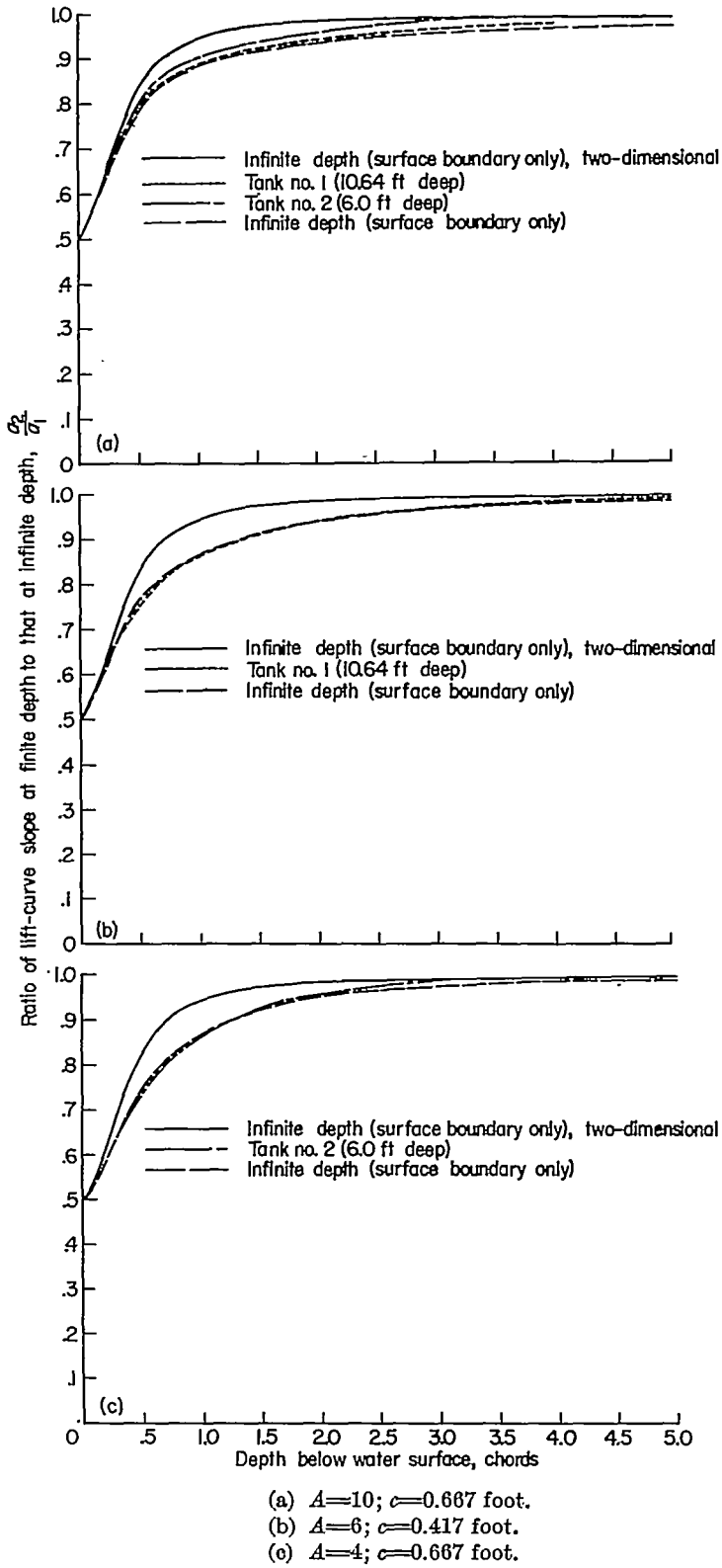

(a) A=10; c=0.667 foot.
(b) A=6; c=0.417 foot.
(c) A=4; c=0.667 foot.

FIGURE 14.—Effect of depth of submergence on lift-curve slope.

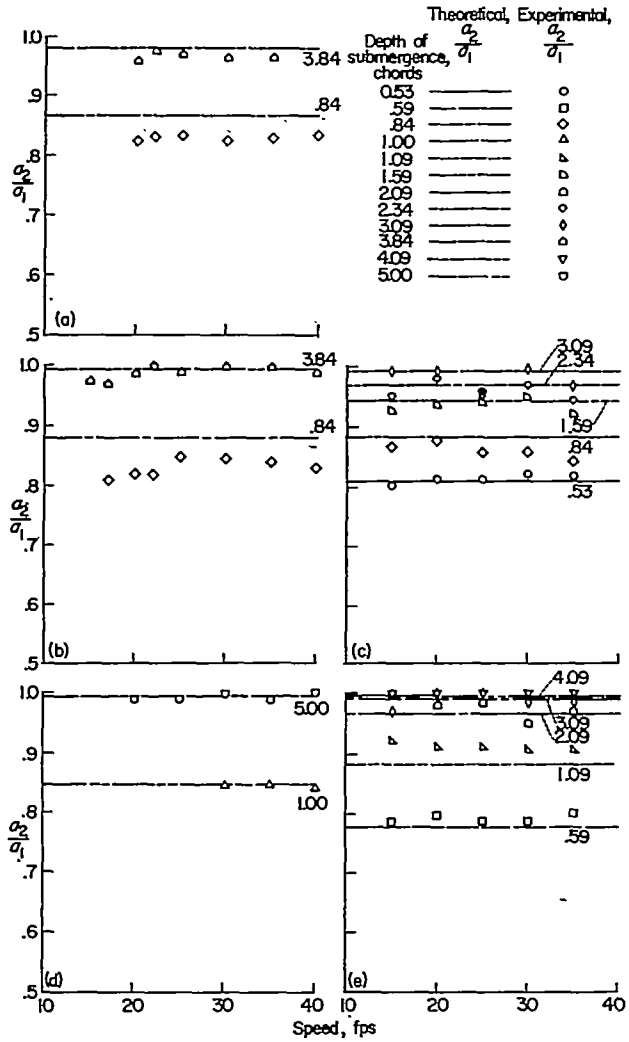

(a) A=10; tank no. 1.
(b) A=10; tank no. 2.
(c) A=10; tank no. 2 (ref. 8).
(d) A=6; tank no. 1 (ref. 9).
(e) A=4; tank no. 2.

FIGURE 15.—Comparison of experimental and theoretical ratio of lift-curve slopes for aspect ratios 10, 6, and 4.

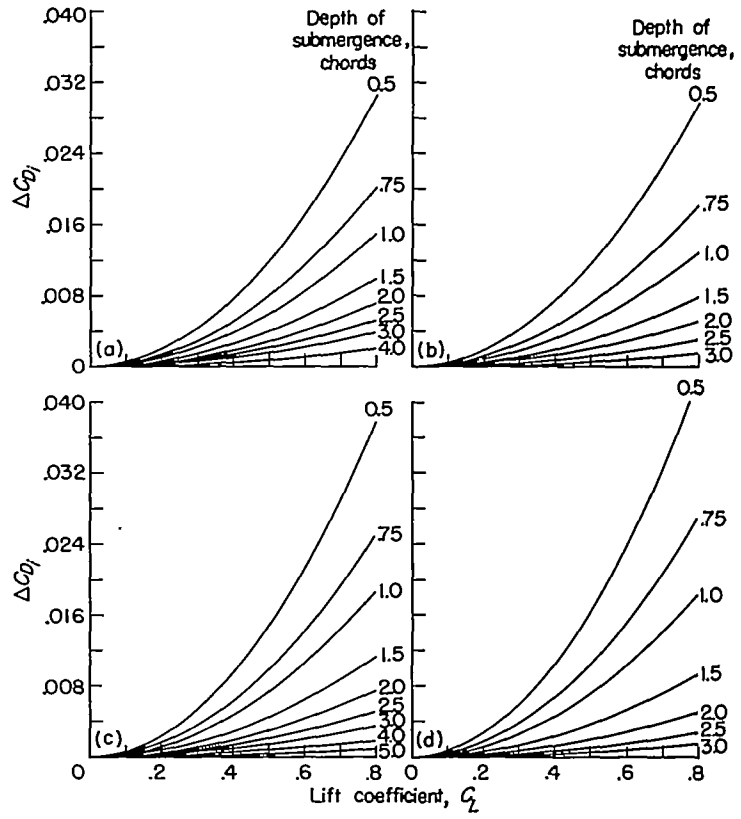

(a) A=10; tank no. 1.
(b) A=10; tank no. 2.
(c) A=6; tank no. 1.
(d) A=4; tank no. 2.

FIGURE 16.—Variation of induced-drag coefficient due to the hydrofoil vortex images with lift coefficient for hydrofoils of aspect ratios 10, 6, and 4.

ratio was chosen for the aspect-ratio-4 hydrofoil because the experimental lift-curve slope at the greatest depth of submergence was approximately 5 percent higher than the lift-curve slope (corrected for aspect ratio by eq. (1)) given by airfoil data. If the method used for the hydrofoils of aspect ratios 6 and 10 had been used, the ratios would be greater than 1.0.

The agreement of the experimental results with results given by the theoretical method is generally good.

Drag.—Results calculated by the restricted-area theoretical method for estimating the effect of depth of submergence on the drag coefficient are shown in figure 16 for hydrofoils of aspect ratios 10, 6, and 4. The magnitude of the increments indicates that a correction to airfoil drag coefficients must be made to predict hydrofoil characteristics at supercritical speeds.

Results calculated by the restricted-area method for both tank no. 1 and tank no. 2 are compared in figure 17 with the present experimental results for a hydrofoil of aspect ratio 10. Figures 18, 19, and 20 present similar comparisons for hydrofoils of aspect ratios 10, 6, and 4; the experimental data for the aspect-ratio-10 and aspect-ratio-6 hydrofoils were obtained from references 8 and 9, respectively, and the experimental data for the aspect-ratio-4 hydrofoil are presented herein. The agreement of the experimental results with results given by the theoretical method is in most cases good.

THEORETICAL BOUNDARY CORRECTIONS—SUBCRITICAL

GENERAL

The speed of propagation of the transverse waves generated by the bound vortex of the hyrdofoil is limited to a speed which is a function of water depth. This speed is defined by $\sqrt{gh}$ where g is the gravitational constant and h is the water depth. When the hydrofoil operates below this limiting or critical speed, the transverse waves travel along with the hydrofoil, whereas above this speed the transverse waves no longer accompany the hydrofoil. It follows, therefore, that the induced effects on lift and drag due to these waves are present below critical speeds but not above. The diverging waves due to the trailing vortices are not subject to this limitation and their effect is present at both subcritical and supercritical speeds. The effect, then, of the trailing vortices can be computed to a first approximation in the same manner at subcritical and supercritical speeds. The effect of the bound vortex at subcritical speeds, however, is not the same as at supercritical speeds.

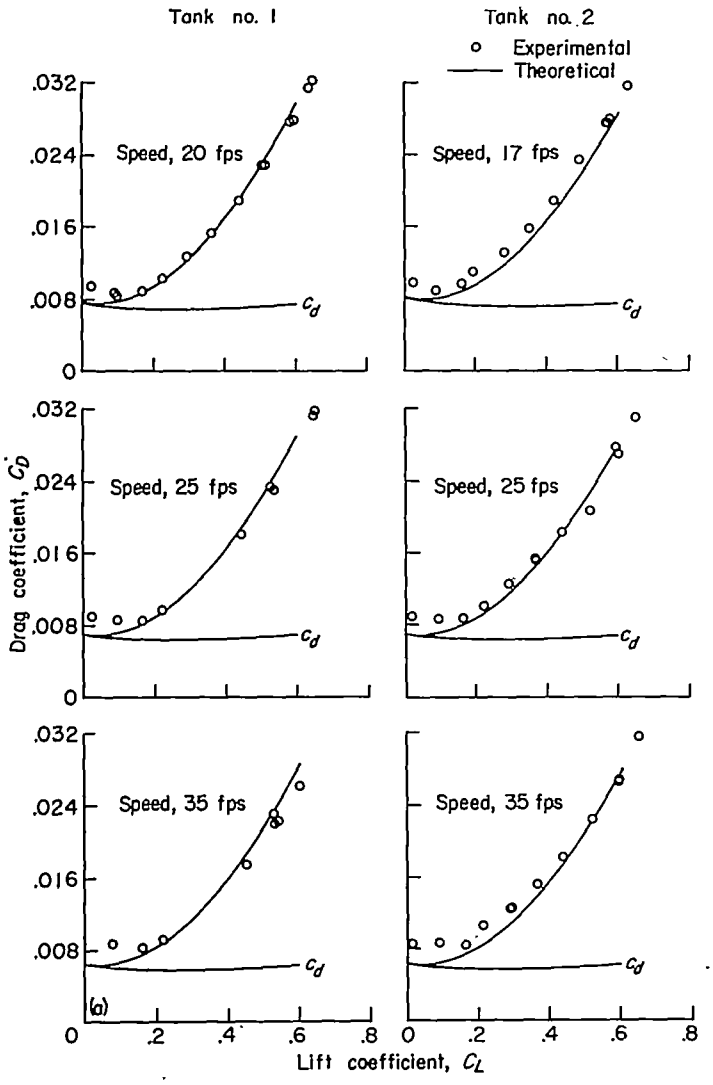

(a) Depth of submergence, 0.84 chord.

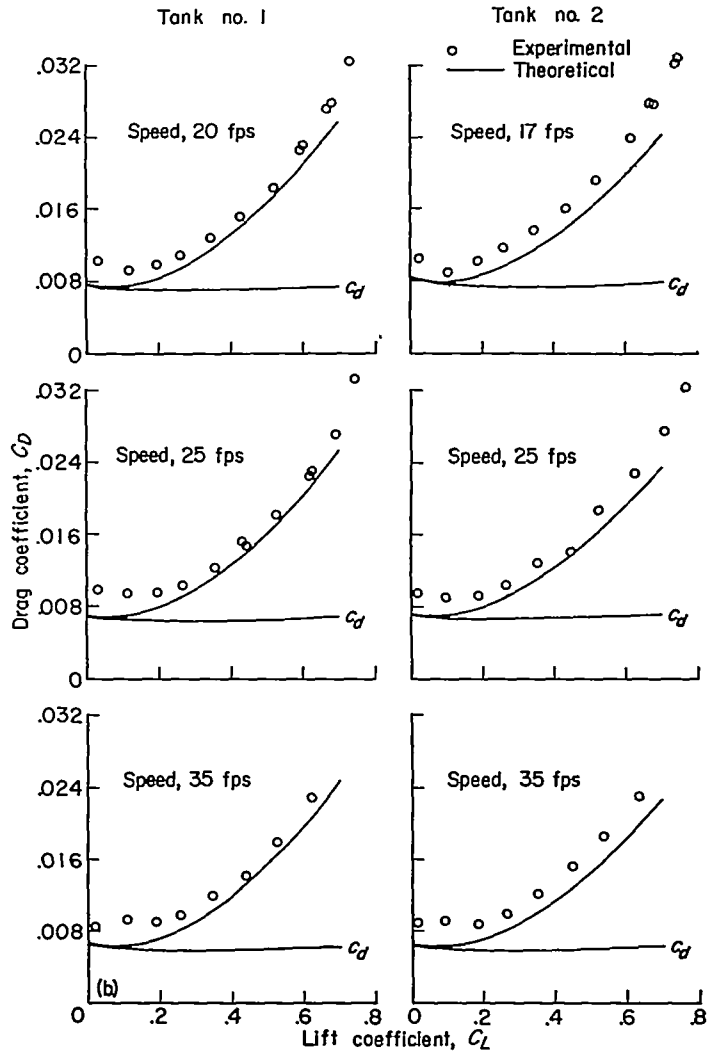

(b) Depth of submergence, 3.84 chords.

FIGURE 17.—Comparison of experimental and theoretical drag coefficients for aspect-ratio-10 hydrofoil.

FIGURE 17.—Concluded.

Figure 10 indicates that the expected effect of the critical speed on lift was either not present or so small as to be masked by the Reynolds number effects encountered in the tests and by the effects of submergence. It can therefore be assumed that to a first approximation the influence of the boundaries on lift will be the same as for the supercritical case and that only the influence on drag need be considered.

Since the condition generally encountered in actual applications is that of great water depth, most of the theoretical work has considered only this case. Mathematical investigations of the wave drag of a submerged body were made by Lamb, who studied the motion of a circular cylinder and a spherical body. More exact solutions of these problems were given by Havelock, who solved further problems, for instance, that of the motion of a submerged ellipsoid. L. N. Sretensky (ref. 12) approached the problem of the submerged cylinder for both infinite and finite water depths by assuming the existence of circulation. Kotchin (ref. 13) gave general formulas for the hydrodynamic forces acting on profiles of arbitrary shape in water of infinite depth. Vladimirov (ref. 14) considered the case of a three-dimensional hydrofoil in water of infinite depth. Meyer in reference 15 considered a two-dimensional hydrofoil in both infinite and finite water depths and in reference 16 considered the case of a three-dimensional hydrofoil in water of infinite depth.

DRAG

In order to estimate the effect of depth of submergence on drag, the induced drag due to the hydrofoil trailing-vortex images and wave drag must be added to the drag in an infinite fluid.

The boundary-induced-drag coefficient due to the image trailing vortices is

$$\delta C_{D_i}=C_L\frac{W_4}{V}(1+\sigma) \tag{14}$$

From equation (5)

$$\frac{W_4}{V}=\frac{\Gamma}{4\pi V}K_1$$

where, for a free surface,

$$K_1=\frac{2s}{s^2+(2f)^2}\left[\frac{c}{2\sqrt{s^2+(2f)^2+\left(\frac{c}{2}\right)^2}}+1\right]$$

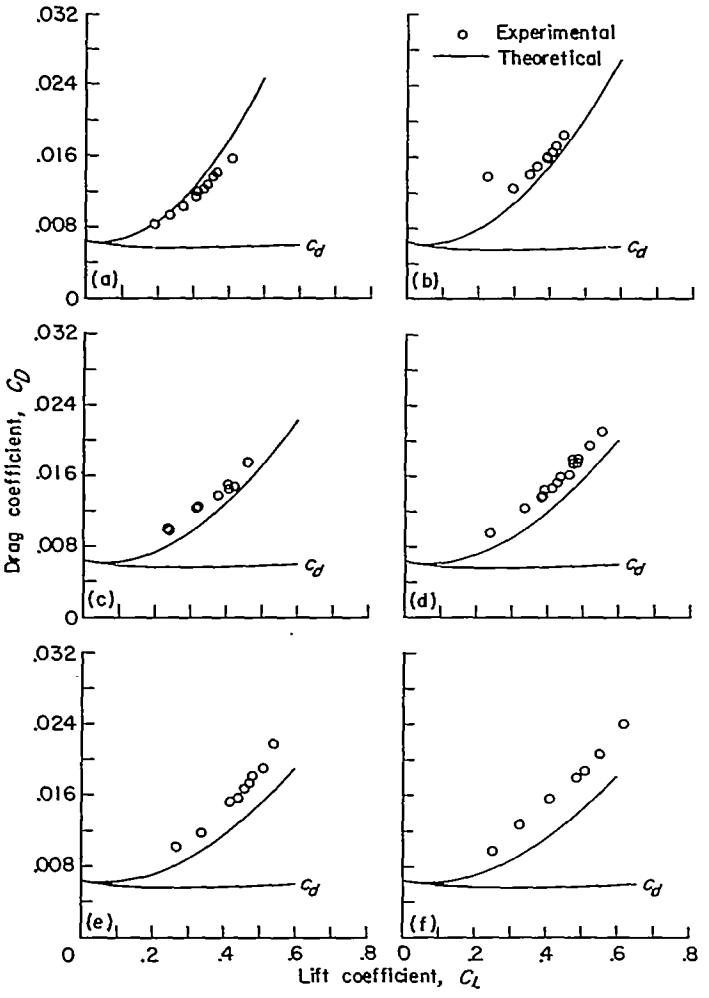

(a) Depth of submergence, 0.53 chord.
(b) Depth of submergence, 0.84 chord.
(c) Depth of submergence, 1.59 chords.
(d) Depth of submergence, 2.34 chords.
(e) Depth of submergence, 3.09 chords.
(f) Depth of submergence, 3.84 chords.

FIGURE 18.—Comparison of experimental and theoretical drag coefficients for aspect-ratio-10 hydrofoil (see ref. 8). Speed, 25 fps.

and from equation (13), for a restricted area (tank no. 1 and tank no. 2),

$$K_1=\frac{y+s}{z^2+(y+s)^2}\left[1+\frac{x}{\sqrt{x^2+z^2+(y+s)^2}}\right]-\frac{y-s}{z^2+(y-s)^2}\left[1+\frac{x}{\sqrt{x^2+z^2+(y-s)^2}}\right] \tag{15}$$

The wave-drag coefficient for a hydrofoil at a given depth of submergence and speed is (refs. 13, 15, and 16)

$$C_{D_3}=\frac{C_{L_2}^2}{2\frac{V^2}{gc}}\psi \tag{16}$$

where, for a two-dimensional hydrofoil in water of infinite depth (refs. 13 and 15)

$$\psi=e^{-2/F} \tag{17}$$

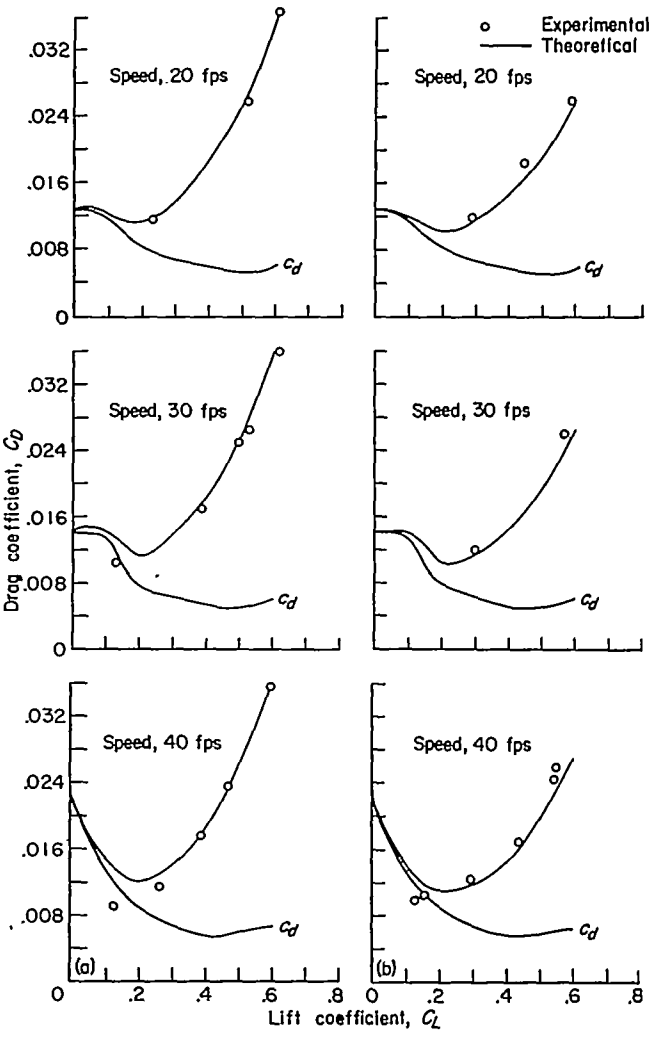

(a) Depth of submergence, 1.0 chord.
(b) Depth of submergence, 5.0 chords.

FIGURE 19.—Comparison of experimental and theoretical drag coefficients for aspect-ratio-6 hydrofoil (see ref. 9).

for a two-dimensional hydrofoil in water of finite depth (ref. 15)

$$\psi=\frac{\sinh^2\left[\left(1-\frac{f}{h}\right)U_0\right]}{\cosh^2 U_0-\frac{gh}{V^2}} \tag{18}$$

(the parameter U_0 is obtained from the relations $\frac{V^2}{gh}=\frac{\tanh U_0}{U_0}$), and for a three-dimensional hydrofoil in water of infinite depth (ref. 16)

$$\psi=\frac{V^2}{gs}\int_{\Lambda_2=-\frac{s}{f}}^{\frac{s}{f}} d\Lambda_2\int_{\Lambda_1=-\frac{2s}{f}}^{\frac{2s}{f}}\psi_2\left(F,\ \text{arc tan}\ \frac{\Lambda_1}{2}\right)d\Lambda_1 \tag{19}$$

where

$$\psi_2(F,\theta)=\frac{1}{32}\left\{\frac{e^{-\frac{1}{F}}}{F^2}\left[(1+\cos^2\theta)\,iH_0^{(1)}\left(\frac{i}{F\cos\theta}\right)\right]-(2\cos\theta+F\cos\theta\cos 2\theta)H_1^{(1)}\left(\frac{i}{F\cos\theta}\right)-\frac{\cos^2\theta\cos 2\theta}{\pi}\right\}$$

$$\theta=\text{arc tan}\left(\frac{s}{2f}\right)$$

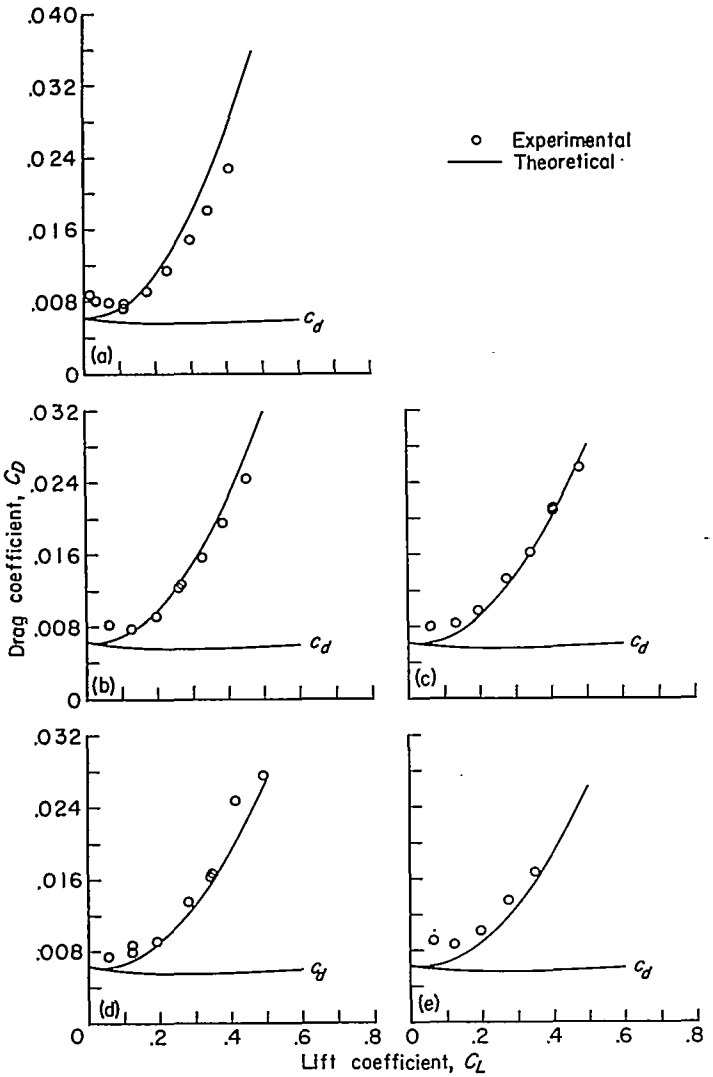

(a) Depth of submergence, 0.59 chord.
(b) Depth of submergence, 1.09 chords.
(c) Depth of submergence, 2.09 chords.
(d) Depth of submergence, 3.09 chords.
(e) Depth of submergence, 4.09 chords.

FIGURE 20.—Comparison of experimental and theoretical drag coefficients for aspect-ratio-4 hydrofoil. Speed, 25 fps.

and $H_0^{(1)}$ and $H_1^{(1)}$ are Hankel functions.

The drag coefficient of a rectangular hydrofoil in an infinite fluid is

$$C_{D_1}=c_d+\frac{C_{L_1}^2}{\pi A}(1+\sigma) \tag{20}$$

The total drag coefficient of a rectangular hydrofoil at a given depth of submergence, angle of attack, and speed is

$$C_{D_2}=c_d+C_{L_2}^2\left[\frac{1+\sigma}{\pi A}+\frac{K_1 c(1+\sigma)}{8\pi}+\frac{1}{2\dfrac{V^2}{gc}}\psi\right] \tag{21}$$

COMPARISON OF THEORY AND EXPERIMENT

Figures 21 and 22 compare the present experimental results for a hydrofoil of aspect ratio 10 with the results calculated from equation (21). The theoretical results were obtained by estimating the second drag coefficient c_d and by adding

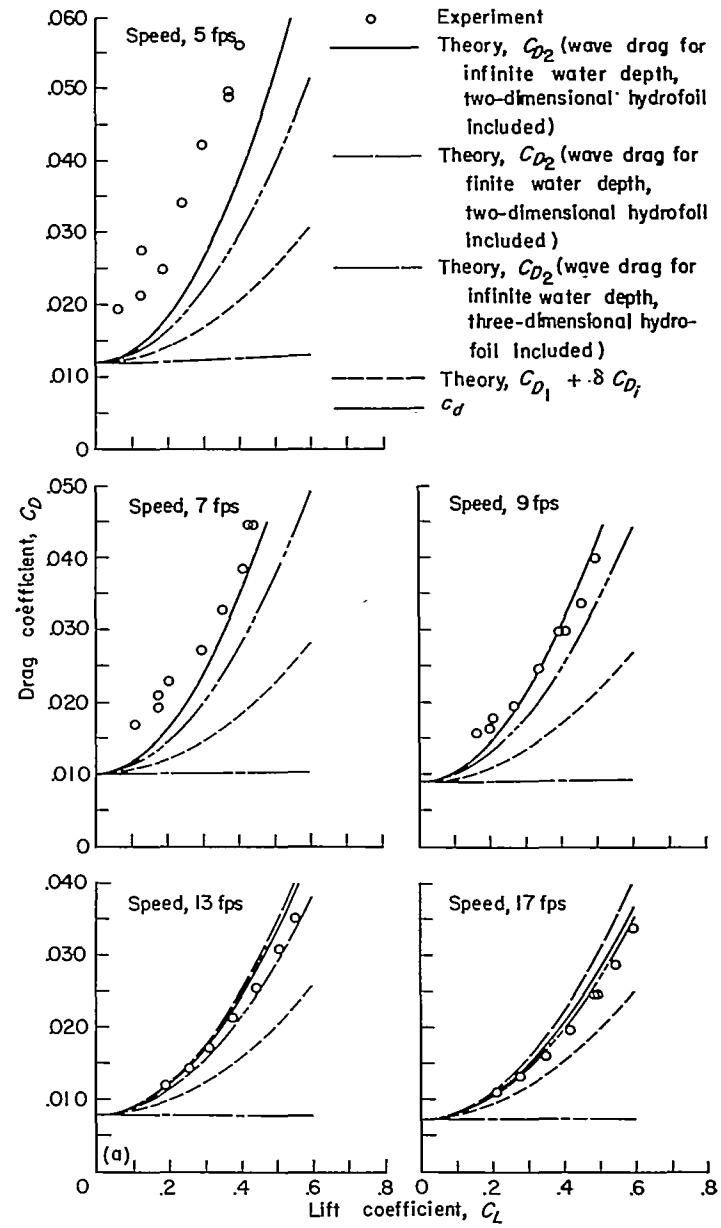

(a) Depth of submergence, 0.84 chord

FIGURE 21.—Comparison of experimental and theoretical drag coefficients for aspect-ratio-10 hydrofoil. Water depth, 10.64 feet (tank no. 1).

the calculated induced-drag coefficient of a rectangular hydrofoil in an infinite fluid C_{D_i}, the boundary-induced-drag coefficient δC_{D_i}, and the wave-drag coefficient C_{D_3}.

The section drag coefficient c_d at low Reynolds number was estimated by extending the section drag data of the NACA 64_1–412 airfoil by comparison (fig. 23) with low Reynolds number data for the NACA 65_3–418 airfoil section. The boundary-induced-drag coefficient δC_{D_i} (eq.(14)) was obtained by calculating K_1 for tank no. 1 and K_1 for tank no. 2 from equation (15). The wave-drag coefficient was computed from equation (16), where the values for ψ were calculated from equation (17) (infinite water depth, two-dimensional hydrofoil), equation (18) (finite water depth, two-dimensional hydrofoil), and equation (19) (infinite water depth, three-dimensional hydro-

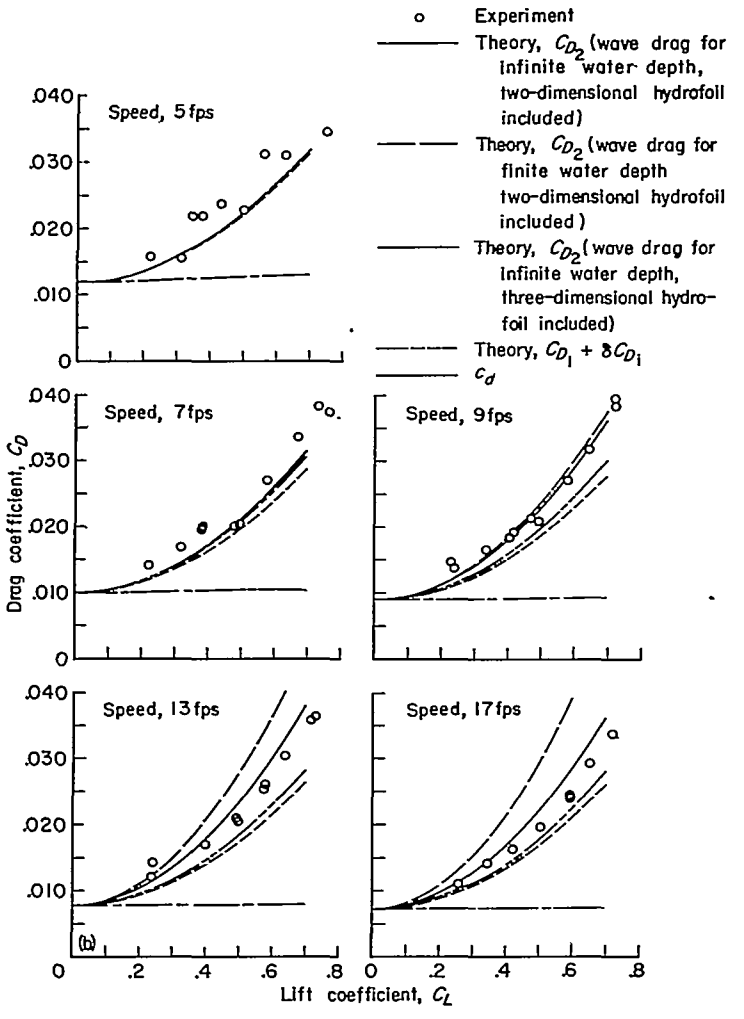

(b) Depth of submergence, 3.84 chords.

FIGURE 21.—Concluded.

foil). The values for ψ obtained from equations (17), (18), and (19) are compared in figure 24.

Figures 21 and 22 indicate that the wave-drag coefficient for water of infinite depth (two-dimensional hydrofoil) added to $C_{D_1}+\delta C_{D_i}$ where $C_{D_1}=c_d+C_{D_i}$ gives a better approximation of the experimental drag coefficient of a hydrofoil at a given depth of submergence and speed than when wave drag is calculated for water of finite depth (two-dimensional hydrofoil) or for water of infinite depth (three-dimensional hydrofoil).

This result may be due to the fact that the wave-drag theories do not consider both the effect of water depth and the three-dimensional case simultaneously, whereas the experimental values were at a finite water depth for an aspect-ratio-10 hydrofoil. Suitable experimental data for other aspect ratios and water depths are not now available to aid in clarifying the discrepancy. The difference in the theoretical and experimental results at 5 fps could be an additional section drag increment since the section drag coefficient was estimated by an arbitrary method.

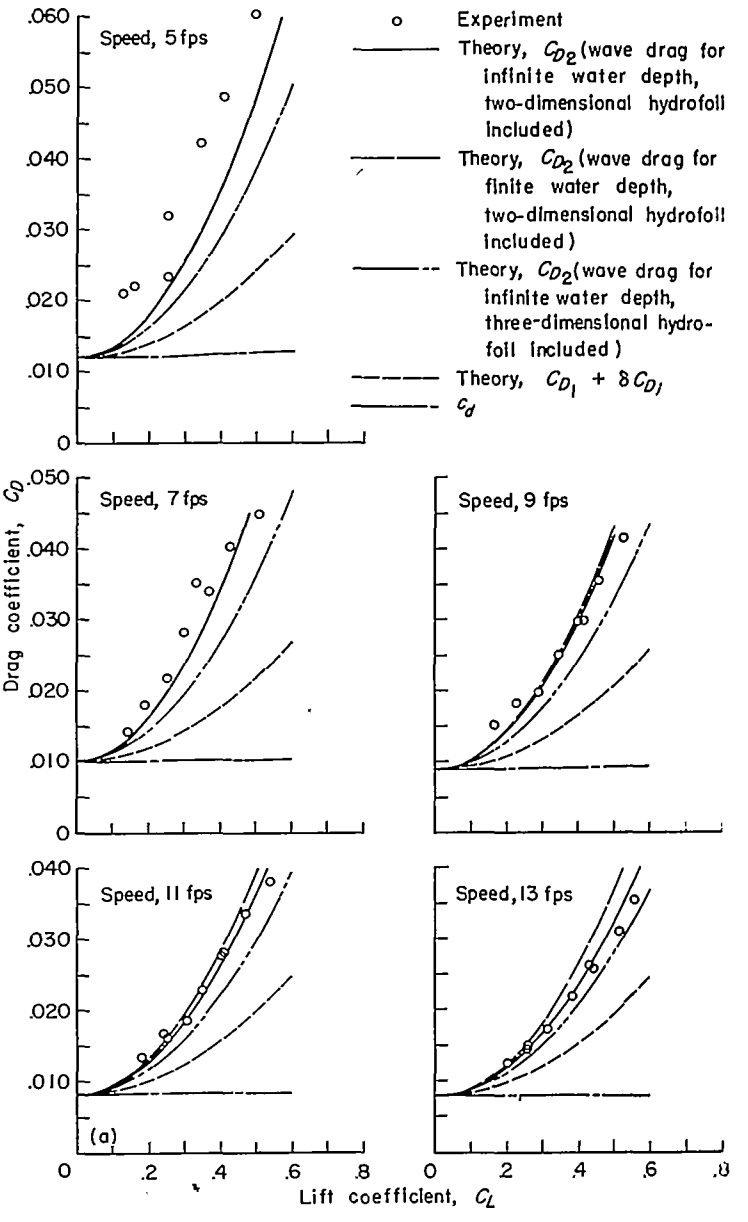

(a) Depth of submergence, 0.84 chord.

FIGURE 22.—Comparison of experimental and theoretical drag coefficients for aspect-ratio-10 hydrofoil. Water depth, 6.0 feet (tank no. 2).

CONCLUSIONS

A comparison of the results calculated by theory and those obtained experimentally for hydrofoils having aspect ratios of 6 (presented in NACA WR L-758) and 4 at supercritical speeds and an aspect ratio of 10 at subcritical and supercritical speeds may be summarized as follows:

1. A method has been developed which makes it possible to calculate at subcavitation speeds, to engineering accuracy, the lift and drag characteristics of a hydrofoil from aerodynamic data. The method accounts for the effects of submergence of the hydrofoil below the free-water surface, the proximity of fixed boundaries, and the limiting speed of wave propagation due to limited water depth.

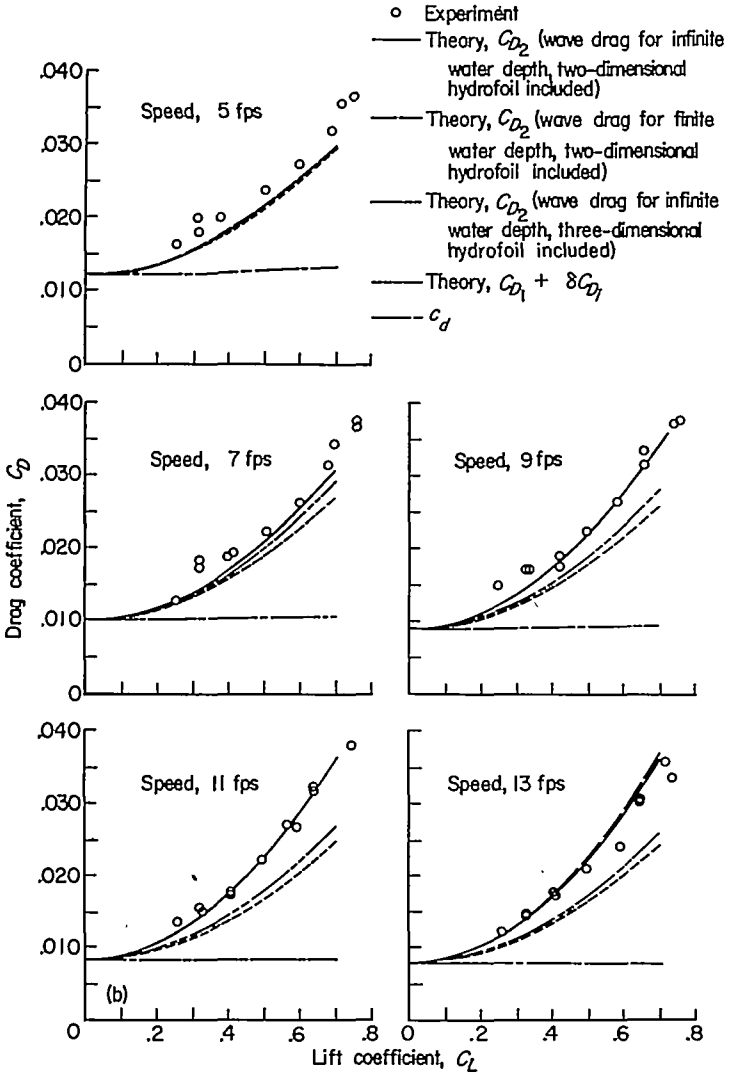

(b) Depth of submergence, 3.84 chords.

FIGURE 22.—Concluded.

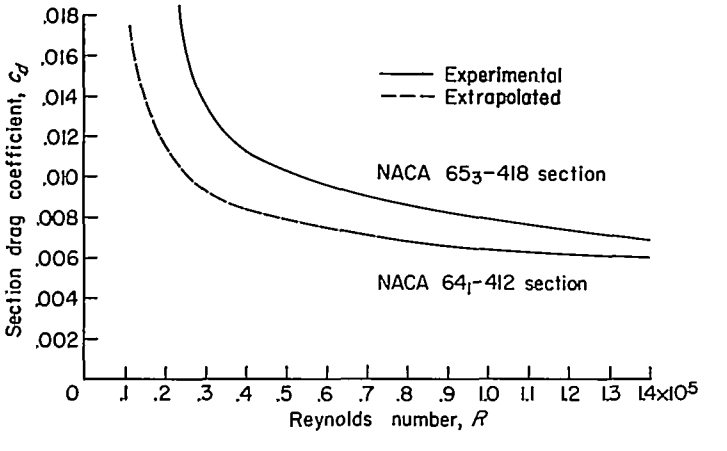

FIGURE 23.—Variation of section drag coefficient with Reynolds number (C_L=0.2).

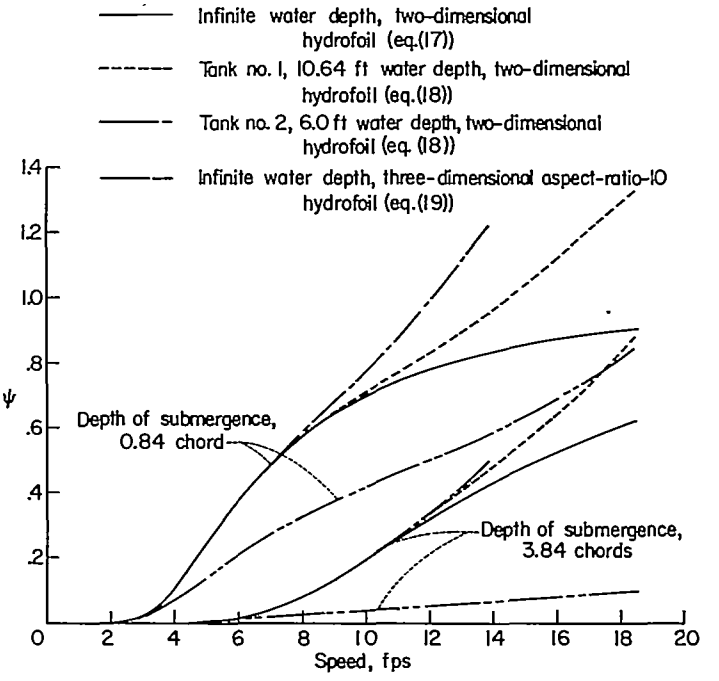

FIGURE 24.—Variation of ψ (see eq. (16)) with speed for infinite water depth and for finite water depth at 0.84 and 3.84 chords hydrofoil submergence.

2. There was no appreciable effect of the limiting speed of wave propagation on lift-curve slope or angle of zero lift at the two depths of submergence investigated.

3. The increase in drag as the critical speed is approached from the supercritical range is gradual. This result is contrary to the abrupt increase at the critical speed predicted by theory.

LANGLEY AERONAUTICAL LABORATORY,
NATIONAL ADVISORY COMMITTEE FOR AERONAUTICS,
LANGLEY FIELD, VA., *April 22, 1952.*

REFERENCES

1. Loftin, Laurence K., Jr.: Theoretical and Experimental Data for a Number of NACA 6A-Series Airfoil Sections. NACA Rep. 903, 1948. (Supersedes NACA TN 1368.)
2. Abbott, Ira H., Von Doenhoff, Albert E., and Stivers, Louis S., Jr.: Summary of Airfoil Data. NACA Rep. 824, 1945. (Supersedes NACA WR L-560.)
3. Quinn, John H., Jr., and Tucker, Warren A.: Scale and Turbulence Effects on the Lift and Drag Characteristics of the NACA 65_3-418, a=1.0 Airfoil Section. NACA WR L-138, 1944. (Formerly NACA ACR L4H11.)
4. Swanson, Robert S., and Crandall, Stewart M.: Lifting-Surface-Theory Aspect-Ratio Corrections to the Lift and Hinge-Moment Parameters for Full-Span Elevators on Horizontal Tail Surfaces. NACA Rep. 911, 1948. (Supersedes NACA TN 1175.)
5. Swanson, Robert S., and Priddy, E. LaVerne: Lifting-Surface-Theory Values of the Damping in Roll and of the Parameter Used in Estimating Aileron Stick Forces. NACA WR L-53, 1945. (Formerly NACA ARR L5F23.)
6. Wieghardt, Karl: Chordwise Load Distribution of a Simple Rectangular Wing. NACA TM 963, 1940.

7. Glauert, H.: The Elements of Aerofoil and Airscrew Theory. Second ed., Cambridge Univ. Press, 1947 (Reprinted 1948).
8. Wadlin, Kenneth L., Ramsen, John A., and McGehee, John R.: Tank Tests at Subcavitation Speeds of an Aspect-Ratio-10 Hydrofoil With a Single Strut. NACA RM L9K14a, 1950.
9. Benson, James M., and Land, Norman S.: An Investigation of Hydrofoils in the NACA Tank. I—Effect of Dihedral and Depth of Submersion. NACA WR L-758, 1942. (Formerly NACA ACR, Sept. 1942.)
10. Stack, John: Tests of Airfoils Designed to Delay the Compressibility Burble. NACA Rep. 763, 1943. (Supersedes NACA TN 976.)
11. Loftin, Laurence K., Jr., and Smith, Hamilton A.: Aerodynamic Characteristics of 15 NACA Airfoil Sections at Seven Reynolds Numbers From 0.7×10^6 to 9.0×10^6. NACA TN 1945, 1949.
12. Sretensky, L. N.: Motion of a Cylinder Under the Surface of a Heavy Fluid. NACA TM 1335, 1952.
13. Kotchin, N. E.: On the Wave-Making Resistance and Lift of Bodies Submerged in Water. Tech. and Res. Bull. No. 1–8, Soc. Naval Arch. and Marine Eng., Aug. 1951.
14. Vladimirov, A. N.: Approximate Hydrodynamic Design of a Finite Span Hydrofoil. NACA TM 1341, 1955.
15. Meyer, Rudolf X.: Two-Dimensional Vortex-Line Theory of a Hydrofoil Operating in Water of Finite Depth. Tech. Rep. HR–1, The Hydrofoil Corp., Nov. 29, 1950.
16. Meyer, R. X.: Three-Dimensional Vortex-Line Theory of a Hydrofoil Operating in Water of Large Depth. Part I: The Wave Drag of a Single Hydrofoil With Prescribed Lift-Distribution. Tech. Rep. HR–4, The Hydrofoil Corp., Feb. 7, 1951.

TABLE I.—ORDINATES OF STRUT AND HYDROFOIL

Stations and ordinates are given in inches

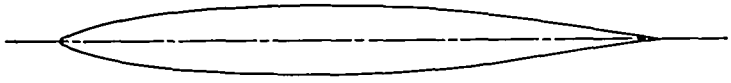

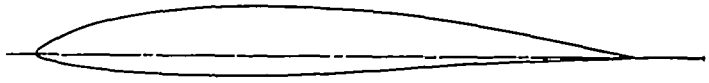

Strut, NACA 66I-012

Station	Ordinate
0	0
.040	.072
.060	.087
.100	.109
.200	.145
.400	.200
.600	.243
.800	.280
1.200	.339
1.600	.384
2.000	.419
2.400	.445
2.800	.464
3.200	.476
3.600	.480
4.000	.477
4.400	.467
4.800	.447
5.200	.411
5.600	.361
6.000	.301
6.400	.236
6.800	.167
7.200	.099
7.600	.038
8.000	0

L.E. radius: 0.076

Hydrofoil, NACA 64$_1$A412

Upper surface		Lower surface	
Station	Ordinate	Station	Ordinate
0.026	0.084	0.054	−0.067
.044	.104	.076	−.079
.082	.135	.118	−.096
.179	.194	.221	−.126
.376	.279	.424	−.164
.575	.346	.625	−.190
.775	.401	.825	−.211
1.176	.490	1.224	−.241
1.578	.559	1.622	−.261
1.981	.611	2.019	−.274
2.384	.648	2.416	−.281
2.788	.673	2.812	−.281
3.191	.684	3.209	−.275
3.595	.679	3.605	−.259
3.999	.661	4.001	−.236
4.402	.632	4.398	−.207
4.805	.592	4.795	−.176
5.208	.544	5.192	−.142
5.610	.487	5.590	−.108
6.012	.422	5.988	−.076
6.414	.349	6.386	−.050
6.814	.265	6.786	−.034
7.210	.179	7.190	−.022
7.605	.090	7.595	−.012
8.000	.002	8.000	−.002

L.E. radius: 0.083
Slope of radius through L.E.: 0.168